kinases and phosphatases

MDPI

Article

Quaternary Protein Model of the Barley MKK3 Enzyme in Complex with Its Candidate Upstream MAP3K Kinase and Functional Implications

Maria Hrmova [1,*], Julian G. Schwerdt [1,2] and Geoffrey B. Fincher [1,†]

[1] School of Agriculture, Food and Wine, Waite Research Institute, Adelaide University, Waite Campus, Glen Osmond, SA 5064, Australia; julian.schwerdt@adelaide.edu.au (J.G.S.); geoffrey.fincher@adelaide.edu.au (G.B.F.)
[2] Plant Synthetic Biology Australia, School of Agriculture, Food and Wine, Adelaide University, Waite Campus, Glen Osmond, SA 5064, Australia
* Correspondence: maria.hrmova@adelaide.edu.au
† Dedication: The co-authors dedicate this work to Professor Geoffrey B. Fincher on the occasion of his 80th birthday and in recognition of his pioneering contributions to plant sciences that helped to advance this field.

Abstract

The mitogen-activated protein kinase (MAPK) cascade is crucial in transmitting extracellular signals to the nucleus, where transcriptional patterns are adjusted in response to changing environmental conditions. In barley, a specific cascade enzyme, MKK*3*, mediates the duration of dormancy and hence the subsequent germination of the grain. Higher activity of this *Hv*MKK3 isoenzyme is associated with decreased grain dormancy, but also with increased risks of yield losses through pre-harvest sprouting of the grain. Previous work has shown how the MKK3 isoenzyme docks with and phosphorylates its downstream substrate HvMAPK. Here, we used computational, analytical and phylogenetic methods to generate a quaternary structural model of the barley MKK3 enzyme with its candidate upstream MAP3K, working as a structurally consistent complex. Although this model awaits confirmation, it provides a structural rationale for the binding and subsequent hydrolysis of ATP by MAP3K and the phosphorylation of Thr residues in the downstream MKK3's activation loop. This MAP3K enzyme is encoded by a single highly conserved gene on chromosome 5H in 76 wild and domesticated barley species. Potential functions of conserved protein sequence motifs in intrinsically disordered regions of the enzyme are considered in relation to the activation and turnover of the enzyme.

Keywords: catalytic site mechanism; evolutionary analyses; *Hordeum vulgare*; intrinsically disordered regions; kinase–kinase docking; phosphorylation sites; plant mitogen-activated protein kinases; protein–protein interactions; structure–function relationships

Check for updates

Academic Editor: Mauro Salvi

Received: 28 August 2026
Revised: 21 October 2026
Accepted: 27 October 2026
Published: 31 October 2026

Copyright: © 2026 by the authors. Licensee MDPI, Basel, Switzerland. This article is an open access article distributed under the terms and conditions of the Creative Commons Attribution (CC BY) license.

1. Introduction

Mitogen-activated protein kinases (MAPKs) in plants mediate multiple processes through the phosphorylation and simultaneous activation of a broad range of enzymes and proteins. Specific MAPK enzymes form cascades of successive phosphorylation reactions (Figure 1) that receive external signals, including abiotic and biotic stress signals, hormonal signals and signals that regulate normal plant growth and development, which are subsequently relayed to the nucleus, where appropriate gene expression is initiated [1–3].

In barley (*Hordeum vulgare*), there has been a strong focus on the MAPKK enzyme (designated here as HvMKK3) because of its role in the regulation of the transition from grain

dormancy to germination, where increased activity of the HvMKK3 enzyme is associated with shorter dormancy [4]. In barley, breeders have selected for increased MKK3 activity where end-users in the malting and brewing industries require a length of dormancy that, on the one hand, overcomes the risk of pre-harvest sprouting, which results in yield losses and malting quality downgrading, while on the other hand allowing even and complete germination of a batch of grain during the malting process, after a short storage period. In some countries where plentiful rainfall and mild temperatures prevail during a single year, it is possible to grow two crops of barley each year. In these regions, very short dormancy periods are desirable. Jørgensen et al. [4] showed that *MKK3* gene copy number variation was an important determinant of the length of dormancy of extant barley cultivars, in combination with different haplotypes in which single amino acid residue substitutions at critical sites in the MKK3 alter enzyme activity. Most wild barleys, which usually exhibit longer periods of dormancy, have a single copy of *MKK3*, and in general terms, multiple *MKK3* gene copies and haplotypes that increase enzyme activity are associated with shorter dormancy [4].

Hrmova et al. [5] subsequently used computational and phylogenetic technologies to define a 3D model of the HvMKK3 enzyme in complex with its immediate downstream HvMAPK enzyme. This model allowed the identification of the phosphorylation sites of both enzymes, the residues involved in ATP hydrolysis, the likely position of the released phosphoryl group and a rationale for the effects of residue substitutions in common HvMKK3 genetic variants on HvMKK3 activity and hence on the transition from dormancy to germination.

In the present study, we have used computational, analytical and phylogenetic approaches to define the quaternary structural model of the barley HvMKK3 enzyme with its immediate candidate upstream MAPKKK (designated here as HvMAP3K) enzyme. Both the MKK3 and MAP3K enzymes in plants are encoded by multigene families [6]. For example, the soybean genome contains 38 *MAPK*s, eleven *MKK3*s, and 150 *MAP3K*s [7], the barley Morex v2.0 variant contains 20 *MAPK*s, six *MAPKK*s and 156 *MAP3K*s [8], and the wild and domesticated barley pan-genome assemblies contain seven *MAPKK* and 206 *MAP3K* genes [9]. The wheat genome contains 18 *MAPKK* and 155–156 *MAP3K* genes [10], and the maize genome contains 74 *MAP3K* and 19 *MAPK* genes [1]. There are about 10 putative *mitogen-activated protein kinase kinase kinase kinase* (*MAP4K)* genes in barley, 25 *MAP4K* genes in wheat, 10 in rice and about 11 in maize [3,11]. It must also be noted that not all MAPK enzymes are necessarily involved in cascades of the type shown in Figure 1. While there is a good deal of information on the number and distribution of *MAPK* genes across cereal genomes and on the transcriptional activity of these genes, relatively few studies have been published on the activities of the enzymes. This is not unexpected. Measuring MAPK activity presents complex biochemical challenges.

Following the activation of the upstream MAP4K enzyme from barley, the kinase would be incubated with the purified barley MAP3K enzyme and radioactively γ-labelled ATP, and the phosphorylation of MAP3K would be confirmed. The assay mixture would be optimized for pH and cofactor requirements, followed by the purification of the phosphorylated MAP3K enzyme by gel electrophoresis or affinity chromatography. The activated MAP3K enzyme would next be incubated with the purified MKK3 enzyme and γ-labelled ATP, and the phosphorylation of MKK3 measured. For the calculation of specific activity, the concentration of the enzyme must be accurately determined, and phosphorylation at the expected site would need to be demonstrated. As noted by Hrmova et al. [5], the complexity of the assay would necessitate extensive replication and stringent controls.

Through comparative analyses, we have identified the likely upstream MAP3K kinase in the barley MAPK cascade (Figure 1) and used 3D modeling and docking to generate

a proposed quaternary structure of the MAP3K enzyme with the MKK3 enzyme. The binding site of ATP on the MAP3K enzyme has been identified, together with the residues that catalyze ATP hydrolysis and the transfer of the phosphoryl group to the acceptor hydroxyl group at the activation loop on the MKK3 enzyme. The potential functions of short, conserved protein sequence motifs in intrinsically disordered regions (IDRs) that are located on the N- and C-termini of the catalytic domain of the HvMAP3K enzyme have been proposed, based on experimental and functional data obtained from other widely distributed MAP3K kinases. Together with our previous structural analysis of the MAPK/MKK3 complex [5], the descriptions of the reactions shown in the barley MAPK cascade are now defined (Figure 1). However, it should be noted that MAPK cascade proteins can also phosphorylate cytoplasmic enzymes and other proteins [1] and that MAPK nomenclature across species is not standardized [7,12]. Here, the barley MAPKKK, MAPKK, and MAPK enzymes are referred to in the text as HvMAP3K, HvMKK3 and HvMAPK, respectively (Figure 1).

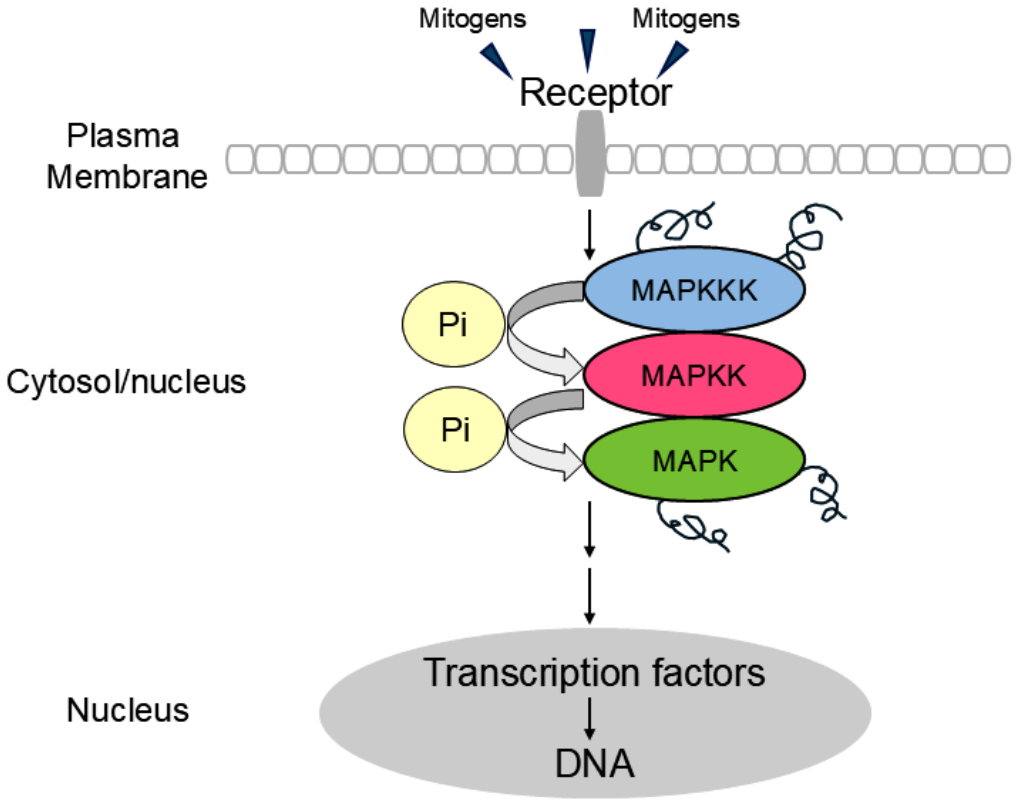

Figure 1. Schematic outline of the mitogen-activated kinase cascade. Following the binding of extracellular mitogens to their plasma membrane-bound receptor, a cascade at each level is initiated in which a mitogen-activated kinase kinase kinase (MAP3K) phosphorylates and activates a mitogen-activated kinase kinase (MAPKK), which in turn phosphorylates and activates a mitogen-activated kinase (MAPK). The activated MAPK subsequently switches on transcription factors in the nucleus. Typically, MAPK cascade proteins contain catalytic modules, additional folded domains, and extended intrinsically disordered regions (IDRs) present in MAPK and MAP3K enzymes. IDRs contain Gly, Ala, Asp, Glu, Pro, and Ser residue-rich regions (shown as random black structureless lines). Redrawn from Wang and Gou [6] and Hrmova et al. [5].

2. Results and Discussion

2.1. Selection of Barley MAP3K for Docking with Barley MKK3

As noted above, MAPK cascade enzymes are encoded by multiple genes and exist in multiple isoforms, not all of which are involved in MAPK cascades [5,8]. As a result, there

are a combinatorially large number of structural possibilities for how two MAPK proteins can interact. Any combination of kinases can be investigated structurally in the MAP kinome. The selection of the HvMAP3K kinase for docking of HvMKK3 was based on the premise that the Arabidopsis MAP3Ks (AtMAP3K17 and AtMAP3K18) [13,14], and the tobacco MAP3K, Nicotiana Protein Kinase 1 (NPK1) [15], all serve as the upstream kinases for MKK3 kinases. Thus, the sequence of NPK1 was subjected to a BLAST search in the UniProt database (https://uniprot.org) (24 January 2026) [16], which resulted in the identification of the barley MAP3K orthologue (accession A0A8I7B904), specifying the full-length sequence of the HvMAP3K kinase of 679 residues (Figure 2; Supplementary Figure S1). The selected HvMAP3K kinase contains the conserved G(T/S)Px(W/Y/F)MAPEV motifs characteristic of the MEKK-like class of kinases [8]. The corresponding accession of the HvMAP3K in GenBank is XP_044946782.1 (https://www.ncbi.nlm.nih.gov/genbank, accessed 1 February 2026), which is identical to A0A8I7B904 listed in the UniProt database. The full-length sequence of barley MKK3 (UniProt accession A0A140JZ13; Supplementary Figure S1), which serves as a substrate for the barley MAP3K, was defined previously [5]. The selection of the HvMAP3K kinases is based on similarity to NPK1 and other MAP3K enzymes known to function upstream of MKK3 in other plant species; however, it remains to be established that it is the biologically relevant upstream kinase to MKK3 in barley.

2.2. Genetics of the Barley MAP3K Gene

Searches of the barley pan-genome database (https://panbarlex.ipk-gatersleben.de; accessed 24 June 2026) [9,17] revealed that the barley *MAP3K* gene identified in Section 2.1 is present as a single copy on chromosome 5H in 76 BPG2 pan-genome assemblies of domesticated, landrace, reference and wild barleys. The gene is in the 415–440 Mbp region of chromosome 5H (Supplementary Figure S2), while the Morex barley *MKK3* gene is in the 583–588 Mbp physical window near the distal tip of chromosome 5H and is under the *SD2* (*Qsd2*) quantitative trait locus (QTL) for grain dormancy [4,18,19]. Both genes are outside the large centromeric 250 Mbp haplotype on chromosome 5H (68.78–320.04 Mbp), which has been under intense recent selection pressure and is characterized by a lack of recombination and high levels of gene fixation [20]. The conservation of the *MAP3K* gene as a single-copy gene at the A0A8I7B904 locus across a large pan-genome collection suggests that *MAP3K* might be a core gene that is of central importance for biological function and plant survival [21].

In view of this core gene possibility and the location of the barley *MAP3K* gene close to the centromeric and pericentromeric regions of highly conserved and fixed genes on chromosome 5H [20], we aligned the 76 MAP3K protein sequences from the barley BPGv2 pan-genome, which includes selected cultivated barley varieties, locally adapted barley *Hordeum vulgare* landraces and a wild *Hordeum spontaneum* line from diverse global growing areas [9,17]. These assemblies include Spring and Winter lines, two-row and six-row lines, hulled and hulless varieties, and exhibit a wide range in the length of dormancy [9,17]. For example, *Hordeum spontaneum* has a relatively long dormancy, as do the FT11 and HOR3942 landraces and the East Asian Akashinriki variety [4]. Other lines in the barley pan-genome (e.g., Morex and Bowman) have low dormancy, and many lines (e.g., RGT Planet) have moderate durations of dormancy [4,9,18] (Supplementary Dataset S1).

The alignments demonstrated that the amino acid sequences in MAP3K enzymes encoded at the A0A8I7B904 locus across the 76 pan-genome assemblies are close to nearly 100% identical. In haplotypes 1, 2, 5 and 6, there is a 34-residue deletion beginning immediately after K132 (Figure 2; Supplementary Figure S1; Supplementary Dataset S1; cf. aligned sequences). A small number of single-residue amino acid substitutions were also detected, such as A100P in haplotypes 3 to 12, and P47A in haplotype 4 and others (Supplementary

Figure S1). The structural analyses (Section 2.5 below) subsequently showed that these two common residue substitutions are unlikely to affect catalysis or complex formation. Several other scattered substitutions were detected in haplotypes 6–12 (Supplementary Dataset S1).

In contrast to the single copy numbers of the highly conserved barley *MAP3K* gene, Jørgensen et al. [4] showed that while wild barley mostly contains a single copy of the *MKK3* gene, domesticated barley varieties and landraces contain up to five tandemly arranged *MKK3* genes, together with diverse DNA sequence haplotypes that are correlated with enzyme activity. They demonstrated that genotypes with certain haplotype combinations and multiple tandemly arranged *MKK*3 genes resulted from anthropogenic or environmental selection that enhanced MKK3 activity and shortened dormancy.

Thus, irrespective of the extreme variations in the duration of dormancy, in the barley pan-genome, all 76 lines have a single *MAP3K* gene at the A0A8I7B904 locus that encodes enzymes with close to 100% sequence identity. It can be concluded that MAP3K does not appear to influence the length of dormancy and that the *MKK3* gene is likely to be a more important determinant of the length of dormancy, despite the participation of both enzymes in the MAPK cascade (Figure 1). The *MKK3* gene is located under the dormancy duration *SD2* QTL, while the *MAP3K* gene is not. Similarly, the *MAP3K* gene is not associated with any particular growth habit characteristic.

2.3. Intrinsically Disordered Regions (IDRs)

The structured functional catalytic domain of the HvMAP3K enzyme consists of 270 residues and is located between an N-terminal intrinsically disordered region (N-IDR) of 95 residues and a 277-residue C-terminal IDR (C-IDR) (Figure 2; Supplementary Figure S3). Gly, Ala, Asp, Glu, Pro, and Ser residue-rich regions are present in both IDRs and are likely to contribute to the absence of defined 3D structure.

IDRs occur in an estimated 70% of eukaryotic proteins [22], including MAP3K enzymes, where their lack of defined structure leaves them exposed and amenable to binding with multiple other regulatory proteins and processing agents [23]. As a result, they can act as switch mediators of regulatory and environmental signaling networks [24–26].

In the past, dynamic interactions of IDRs have proved difficult to evaluate, but the recent development of the FINCHES Intermap tool has enabled predictions of interaction 'hotspots' in IDRs that are broadly distributed in plant and animal organisms [22]. Thus, a possible D-motif in the N-IDR of HvMAP3K could be the RRSINF linear sequence (Figure 2), based on the loosely defined consensus sequence $[R/K]_{1–3}X_{0–2}[\phi]X[\phi]$, where R and K are Arg and Lys, respectively, X is any residue, and ϕ represents a hydrophobic residue; potential D-motifs are found in IDRs from a broad range of MAP3K enzymes [27–31]. Using the FINCHES-online Intermap tool, pretrained on IDRs (https://www.finches-online.com; accessed 24 June 2026) [22], the predicted binding region of the putative RRSINF D-motif in HvMAP3K would be in the N-terminal region of HvMKK3 (CDSYVVSDGGTINLLSRS-FGEYNINEH linear sequence) (Supplementary Figure S1). This sequence folds into an N-terminal loop and a 3-stranded β-sheet with six surface-exposed Asp and Glu residues that may interact with the RRSINF motif (Figure 3). The AlphaFold3-predicted HvMKK3 model has a Local Distance Difference Test (lDDT) score [32] for this region of less than 50%, suggesting that it might contain short, disordered regions and/or flexible segments. Extended IDRs do not appear to be present in MKK3.

C2 protein phosphatases (PP2C) can also bind to the $[K/R_{1–3}X_{1–6}\phi X\phi]$ D-motif of plant MAP3K enzymes via a discontinuous patch of acidic residues on the PP2C. The PP2C enzyme can inactivate the kinase by removing its phosphoryl group from the activation site [33–35]. Alternatively, PP2C, as a negative regulator, can bind to the intracellular abscisic

acid (ABA) receptor PYL, which results in the inactivation of the phosphatase [36,37]. Further complicating these processes is the ability of some MAP3K kinases [38] to be activated by autophosphorylation before the phosphorylation of a downstream kinase [39].

In the HvMAP3K C-IDR, there is a CEDDDVL motif with a Lys (K) residue 19 residues upstream (Figure 2) that is similar to degron docking modules through which a targeted recognition signal directs a protein to the cellular degradation machinery [40,41], and is conserved in related plant MAP3K enzymes (Supplementary Figure S3). The barley MAP3K also has a second potential docking motif, FXFP, in its C-IDR (Figure 2), which is also conserved in related plant MAP3Ks [29] (Supplementary Figure S3). This motif was not detected in MKK3 or downstream MAPK enzymes [5]. It should be emphasized that the specific function of the conserved FXFP and other putative IDR motifs of the barley MAP3K enzyme (Figure 2) is hypothetical and awaits experimental confirmation.

MRRDAAGGPGGGAGFHDLFDSVRRSINFRTSAAAPPEPPAGPLGGGPAGGIGVRISSCLRKSRGMGLLGLISK
SPSPPRRLLPPTPVPADGGGRAGEIPAIRWRKGEMIGSGAFGQVYLGMNLDTGELLAVKQVLIGSTNATREKA
QAHIRELEEEVKLLKNLSHPNIVRYLGTVREEGTLNILLEFVPGGSIQSLLGKLGSFPEAVIRKYTRQILQGL
EYLHSNAIIHRDIKGANILVDNKGCIKLADFGASKQVAKLATMTAAKTMKGTPHWMAPEVIVGSGHTFSADIW
SVGCTVIEMATGKPPWSQQYQEVALLFHVGTTKSHPPIPEHISPEAKDFLLKCLQKEPELRSSASDLLKHPFV
TGEFDDRQLLNRTAQKDASVNELFTHDADAPTEMGLNHSGNWSTINSNRSSKIKPLWEGGGDDDDMCEFADKD
DHRAVGSSYNPMSEPFDDWKSKYDISPEQSSHQSREFGGLAKHAESSMTENDFTFPCEGSCEDDDVLTESKIE
AFLDEKALDLKKLQTPLYEEFYNKVNAGTSHGVDQTSNGKFINSPKLPPRGKSPPGKMRGGSAVATPCDTMFN
SSTMAESCSKQFSRDGVDSSRILREIASPQLNELGDKVHVDVQDSPSISFAERQRKWKEELDQELERERVMRL
AGCGKTPSPSRRPSTGKRERHQ

Figure 2. Full-length sequence of barley NPK1-like MAP3K (UniProt A0A8I7B904/GenBank XP_044946782.1). The structured catalytic domain of 307 residues is shown in green, wherein the catalytic motifs HRD and DFG are highlighted in red font, and the phosphorylation motif (P-motif) is underlined. From this sequence, 270 residues were available for constructing the homology model of HvMAP3K. Candidate phosphorylatable Thr residues are text-highlighted in cyan. The N-IDR of 95 residues preceding the catalytic module is shown in black font and contains the putative RRSINF D-motif (grey) or a putative PP2C (ABI1) docking motif [42]. The 277-residue C-IDR is also shown in black font and includes a possible ubiquitination site with its upstream Lys residue (red), an FTFP binding motif (yellow), together with motifs rich in Gly, Pro, Glu and Asp residues (purple) that are likely to contribute to the disorder of the C-IRD region. Note that the barley MAP3K enzyme does not contain the 34-residue deletion described above (Section 2.2; Supplementary Dataset S1).

In conclusion, although IDRs and common motifs therein have been detected by sequence analyses and structural modelling in the barley MAP3K enzyme (Figures 1 and 2) and even though the functions of these IDR motifs have been confirmed experimentally in many other MAPK enzymes, it must be emphasized again that experimental evidence to support possible interactions of the common IDR motifs in HvMAP3K with other proteins, including MKK3, is currently unavailable.

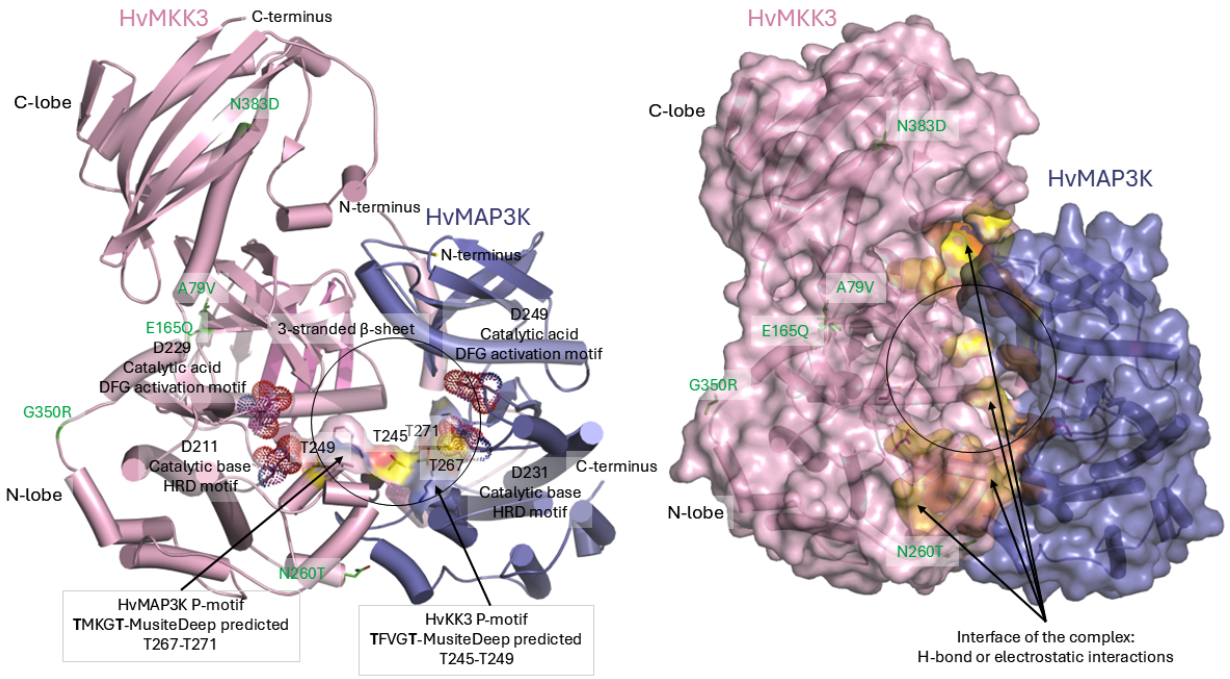

Figure 3. Docking of HvMKK3 into the catalytic module of HvMAP3K. **Left panel**: Cartoon representation of the quaternary model of the HvMAP3K (blue)/HvMKK3 (pink) complex. Catalytic residues D231 (base) and D249 (acid) in HvMAP3K and D211 (base) and D229 (acid) in HvMKK3 are shown in magenta-CPK sticks and dots. The respective phosphorylation sites TMKGT (T267–T271 in HvMAP3K) and TFVGT (T245–T249 in HvMKK3), indicated in blue and pink surface representations, are arranged proximally to allow direct communication. Phosphorylatable T residues in each motif are shown in yellow-CPK sticks. The projected ATP docking site in HvMAP3K is shown by a black circle. Positions of five mutations identified in HvMKK3 [5] are shown in green-CPK sticks. The N-terminal loop and a 3-stranded β-sheet region (magenta) of HvMKK3 that could interact with HvMAP3K are also shown. N- and C-termini of both kinases, and the N- and C-lobes of HvMKK3, are marked. **Right panel**: Surface representation of the HvMAP3K (blue)/HvMKK3 (pink) complex. The cartoon representations show the kinase molecules, with underlying translucent cartoon representations. The interface residues forming hydrogen (H)-bonds or electrostatic interactions in the complex at separations between 2.8 and 3.4 Å, from HvMAP3K and HvMKK3, are shown in respective orange and yellow surface representations. Positions of five mutations identified in HvMKK3 [5] are shown in green-CPK sticks. The projected ATP docking site in HvMAP3K is shown in a black circle.

2.4. Phosphorylation Sites of Barley MAP3K and MKK3

The sequence alignment with MusiteDeep [43] (accessed 24 January 2026) predicted a consensus sequence **T**MKG**T** in HvMAP3K, located in the phosphorylation loop, and that the two Thr (T) residues (bold) in this motif of HvMAP3K are likely to be phosphorylated by a currently unknown upstream kinase (Figures 1 and 3; Supplementary Figure S1). The P-motif **T**FVG**T** of barley MKK3 (UniProt accession A0A140JZ13), which serves as a substrate for barley MKK3, was described previously [5] (Figures 1 and 3; Supplementary Figure S1). These P-motif analyses were confirmed by NetPhos3.1 examination (accessed 24 January 2026) [44].

2.5. Docking of Barley MKK3 into the Catalytic Module of Barley MAP3K

We utilized HDOCK [45], a physics-based computational tool designed for docking and generating protein complexes, as it combines a template-based (using structures of a similar classification) approach to improve the prediction accuracy of protein complexes. This tool provides several hundred models, which can be clustered and evaluated. We used three

criteria to select the most suitable HvMAP3K/HvMKK3 model complex: (i) the mutual orientation of HvMAP3K and HvMKK3 molecules, such that the dispositions of P-sites in the HvMAP3K and HvMKK3 enzymes are proximal; (ii) the disposition of N- and C-termini of kinase molecules in the complex pointing to the surface for potential binding of additional proteins; (iii) interface associations between the HvMAP3K and HvMKK3 enzymes in the complex, which should satisfy stereo-chemical parameters and favorable thermodynamic contacts within 3.5 Å. Meeting these three criteria could provide a plausible mechanistic model for the phosphorylation of the HvMKK3 substrate via phosphoryl diffusion from the hydrolyzed ATP molecule to the acceptor hydroxyl group at the P-site of HvMAP3K [5].

We generated the quaternary HvMAP3K/HvMKK3 structural model of 793 residues in length and determined that the full-length HvMKK3 substrate for HvMAP3K kinase (523 residues) associated favourably with the catalytic module of HvMAP3K (270 residues) (Figures 3 and 4; Supplementary Figure S4). In the favourably docked complex, containing internal cavities (Supplementary Figure S5), HvMKK3 is bound in a cleft facing the surface of HvMAP3K, such that its P-motif **T**FVG**T** (**T**245–**T**249) faces proximally the **T**MKG**T** (T267–T271) motif in HvMAP3K (the two threonine phosphorylatable residues above are in bold letters for both kinases). This orientation of both P-motifs would allow HvMKK3 to be phosphorylated, most likely through the directional diffusion of a P_{γ} phosphoryl group of ATP from the HvMAP3K molecule to HvMKK3. Further, the N- and C-termini of both kinases pointed to the surface of the complex, such that the IDRs of HvMAP3K would be available for binding of additional proteins (Figures 3 and 4). Additional predictions using artificial intelligence (AI)-based docking tools, Chai-1 (accessed 22 August 2026), AlphaFold3 (accessed 30 August 2026) and Boltz-2 (accessed 31 August 2026) confirmed the mutual topology and orientation of both kinase molecules, with RMSD values of 1.34 Å, 1.09 Å and 2.02Å, respectively. These observations reinforced the validity of the HvMAP3K molecule orientation relative to HvMKK3 calculated through docking. However, it must be emphasized that while the detected spatial dispositions of the MAP3K and MKK3 molecules are plausible, the finding is based on the validity of the HvMAP3K/HvMKK3 modelled complex.

Both molecules in the proposed HvMAP3K/HvMKK3 complex together form a tight interaction interface (Figure 3, right panel) shown in yellow- and orange-CPK surface representations for HvMKK3 and HvMAP3K. The PPAP computational tool from the Tamarind Bio suite [46] predicted the binding energy -ΔG −8.8 kcal/mole or the binding affinity (or dissociation) constant K_D 359.3 nM between the two kinases, with the complex buried surface area of 4515 $Å^2$ (using the solvent radius of 1.4 Å). More specifically, 9 residues S111, Q194, H273, K305, Q310, Y312, Q313, E314 and L317 (HvMAP3K) and 11 residues D33, N119, K123, S233, L236, D237, N238, T239, M240, A241 and R257 (HvMKK3), respectively, formed 14 contacts, from which 12 were occupied by H-bonds and two formed ionic pairs at separations between 2.8 and 3.4 Å (Figure 3, right panel). The residues of HvMAP3K formed multiple interface interactions with those of HvMKK3, which together served as a strong foundation for the stable HvMAP3K/HvMKK3 complex. Based on the alignment of 100 sequences (GenBank queried with HvMAP3K or HvMKK3; accessed 8 October 2026), the following interface residues in HvMAP3K were found to be conserved: Q194, K305, Q313, E314, and L317. Additionally, S111, H273, Q310, and Y312 were partially conserved. In comparison, the conserved residues in HvMKK3 included N119, K123, S233, D237, N238, T239, and A241, while D33, L236, T239, and R257 were noted as partially conserved. This proposed model will be subjected to experimental validation in the future, as discussed under Future Directions.

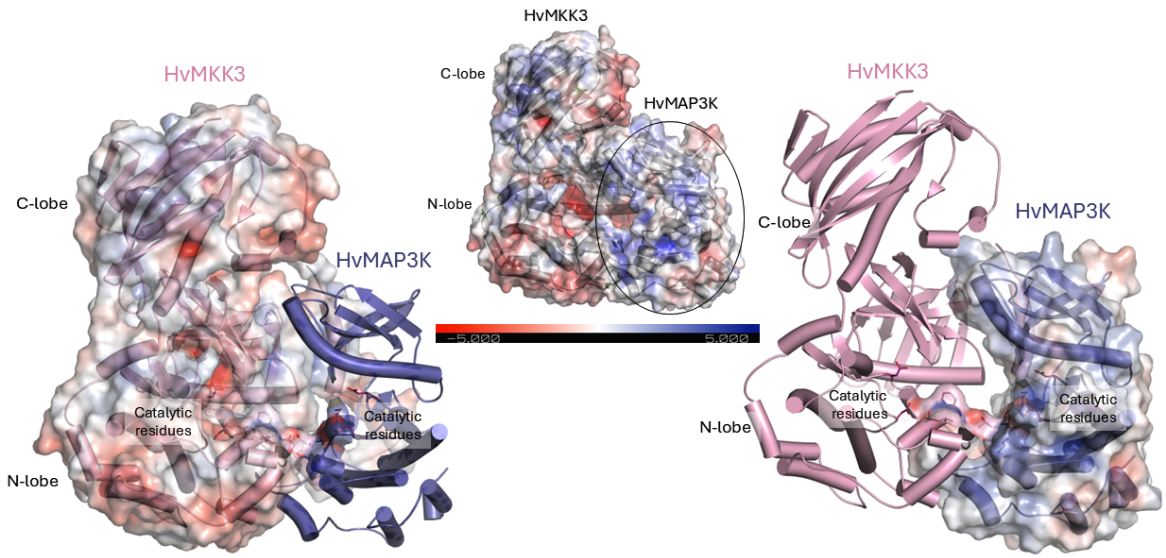

Figure 4. The HvMAP3K/HvMKK3 complex and its electrostatic surface potential. Surface morphology of the quaternary HvMAP3K/HvMKK3 complex molecules coloured by electrostatic potentials with underlying cartoon representations of the HvMAP3K (blue)/HvMKK3 (pink) complex. Electrostatic surface potentials of kinase molecules are visualized jointly (upper image) or separately (left and right large images for HvMAP3K and HvMKK3 molecules, respectively), coloured according to the scales shown on the underlying bar (white for neutral; 5 kTe^{-1} for blue; −5 kTe^{-1} for red). Residues in predicted P-motifs (T267–T271 for TMKGT in HvMAP3K, and T245–T249 for TFVGT in HvMKK3) are shown as blue and pink surface representations and in CPK sticks; they are situated proximally to allow direct communication. Catalytic residues are shown in magenta-CPK sticks.

The surface morphology analysis of the HvMAP3K/HvMKK3 complex, and its interaction interface, coloured by electrostatic potential (Figure 4; scales of white for neutral; +5 kTe^{-1} for blue; −5 kTe^{-1} for red), revealed a balanced charge distribution, without extreme charge contributions from either kinase.

The analysis using InterPro [47] classified the barley MAP3K enzyme within the serine/threonine protein kinase family (TyrPK-CSF1-R group). The full-length HvMAP3K (679 residues) predicted the presence of an intrinsically disordered (or low-complexity) IDR (residues 1–95), including a proline-rich region (residues 75–88), and an ordered catalytic module (residues 102–402), with the remainder of the sequence (residues 403–679) also containing an unassigned structure. The catalytic module (residues 102–401) consists of a coil-coiled region (residues 136–163) and an activation loop (residues 247–273), with the ATP-binding region (residues 204–227), ATP-binding residues V117 and K132, and potential Mg^{2+} binding residues N236 and D249. This analysis also predicted the presence of active site residues (H^+-acceptor D231 of the HRD motif, and H^+-donor D249 of the DFG motif). The predictions via InterPro agreed with the geometry and topology of the calculated HvMAP3K/HvMKK3 complex (Figures 3 and 4).

We applied the HHPred toolkit [48] (20 February 2026) (E-value cutoff 1×10^{-3}) and searched the PDB_mmCIF70_20 domain database [49] with the HvMAP3K catalytic module sequence. Using the HHPred toolkit, we identified 250 structures, mostly of mammalian, bacterial, and fungal origins. A few structures belonged to monocot (*Zea*, *Oryza*) and dicot (*Arabidopsis*, *Medicago*) plant genera. These plant structural homologues included *Zea mays* casein kinase II subunit alpha, *Oryza sativa* chitin elicitor receptor kinase 1, *Medicago trunculata* LYK3 kinase domain D459N, and six *Arabidopsis thaliana* enzymes annotated as serine/threonine-protein, MAP and MAPK kinases. However, they all lacked the required P-motifs homologous to HvMAP3K. These analyses indicated that no known plant MAP3K or its homologues are currently available in structural databases.

As noted above, the protein sequence alignment of the 76-barley pan-genome assemblies showed that a 34-residue insertion occurs in the catalytic domains of haplotypes 20–65 and 71–75 (Supplementary Dataset S1; cf. global alignment). This insertion, namely QVRGFLRFGDLVCAVRRPGVIRHTNSSPLFDFWF, forms a loop or an unstructured region with short α-helices, based on the 3D model we built using the AlphaFold server (using five predictions per seed). This insertion has a 'predicted aligned error' near the insertion region and an lDDT score below 50% [32]. Thus, it is more likely that this insertion will be absent in mature MAP3K enzymes in these haplotypes, as it directly interferes with MAP3K folding and the formation of the HvMAP3K/HvMKK3 complex. This raises the question as to why the majority of the 76 barley lines in the pan-genome do not contain this 34-residue deletion, at least at the DNA level. It is more likely that this 34-residue block is removed through alternative splicing at the RNA level, rather than by proteolytic excision from a translated enzyme.

We next considered whether the common genetic variants in the MKK3 enzyme, which influence its activity and hence the length of dormancy [4], would interfere with the formation of the MAP3K/MKK3 complex. Hrmova et al. [5] defined the positions of the Q165E, N260T, A79V, G350R and N383D variants in the MKK3 enzyme and concluded that the Q165E and N260T variants could directly affect MKK3 activity at the ATP-binding level and at the phosphorylation site, respectively. The A79V, G350R and N383D residues were located 22–43 Å from the catalytic residues D211 and D229. These five MKK3 variants are also distant from the MAP3K/MKK3 complex interface [5] (Figure 3). At the interface of the complex (represented by T267 of MAP3K), the distance between Q165E of MKK3 and T267 is 21 Å, and the distance between N383D of MKK3 and T267 is 37 Å (measured between the Cα atoms of the two residues) (Figure 3). We therefore conclude that these common *MKK3* genetic variants do not interfere with the MAP3K/MKK3 complex formation.

2.6. Docking of ATP into the Barley MAP3K/MKK3 Complex

We docked the ATP molecule into the quaternary structure of the barley MAP3K/MKK3 complex, using AutoDock Vina v1.2.7 [50], focusing on the ligand position presumably located between both molecules. In our theoretical model, we projected the ATP site in HvMAP3K towards HvMKK3 at the interface between both kinase molecules (Figure 3, grey transparent circle). We identified two favourable positions of ATP in the protein complex (Figure 5, left and right images), with comparable binding scores of −6.540 ($K_D = 0.16 \times 10^{-6}$ M) and −5.961 ($K_D = 0.43 \times 10^{-6}$ M) kcal/mol, respectively, based on the thermodynamic equation ΔG = RT ln (K_D) at 298.15 K (25 °C). Based on the coordinates of the complexes with bound ATP, the Small-Molecule Affinity server [51] estimated the following respective $\log_{10}(K_D/K_i)$ values of 10.7 and 9.7 nM for the two AutoDock Vina trials, which we treat as cross-check values. We noticed that AutoDock Vina and the Small-Molecule Affinity server (trained on the PDBbind database, which is a repository linking 3D structural PDB data with experimentally measured binding affinities) showed disagreement between the estimated affinity constants, which stemmed from their different mathematical architectures. While AutoDock Vina relies on a combination of steric interactions, hydrophobic terms, and directional hydrogen bonding (ignoring partial charges and explicit electrostatic components), the Small-Molecule Affinity server utilizes multi-layered descriptors that capture long-range electrostatic grids, π-stacking networks, and quantum-like properties. This implies that estimated K_D values determined by both approaches cannot be compared, as AutoDock Vina prioritizes geometry and a physical pose of a ligand, while the Small-Molecule Affinity server estimates quantitative K_D values.

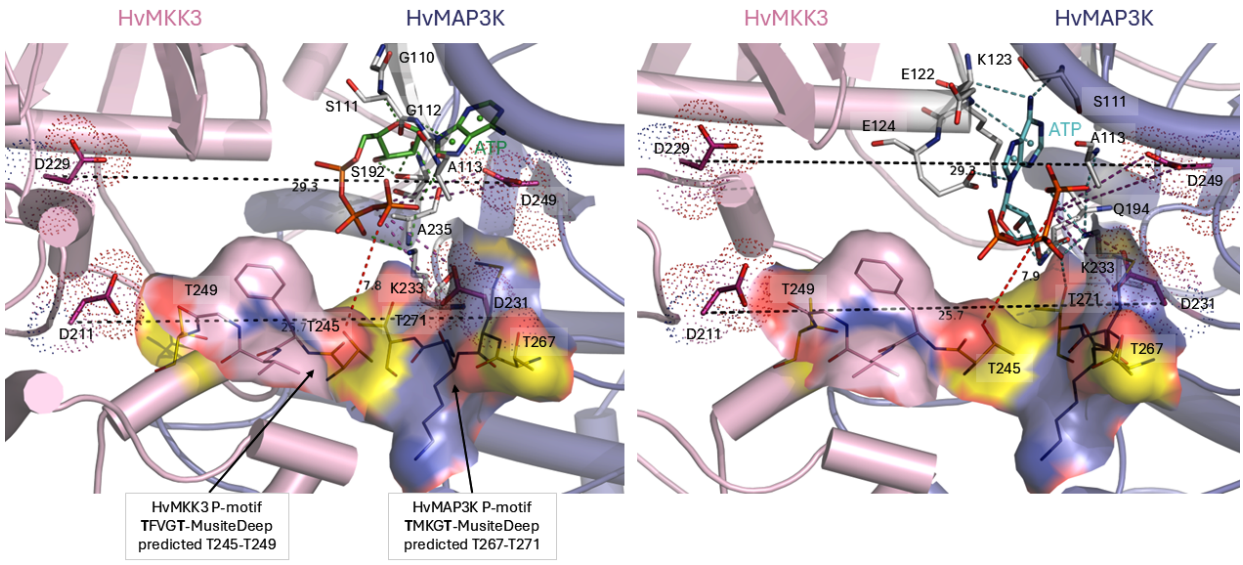

Figure 5. Close-up views of the ATP molecules' interactions in the quaternary HvMAP3K/HvMKK3 complex. Close-up views of cartoon representations of the HvMAP3K (blue)/HvMKK3 (pink) complex with bound ATP are indicated, with positions of ATP molecules (green-CPK and cyan-CPK sticks in the respective left and right images) docked independently in two trials by AutoDock Vina v1.2.7 [50]. Phosphorylatable Thr residues in each P-motif are shown in yellow-CPK lines. Separations between T245 of HvMKK3 and the ATP P_γ phosphate group are indicated in red dashed lines. Separations between interacting residues (grey-CPK sticks) and ATP in each kinase complex, and catalytic residues and the P_γ phosphate groups of ATP molecules are shown in respective green (**left**) or cyan (**right**) dashed lines, and magenta dashed lines. Catalytic residues of kinases in each complex, separated by 29.3 and 25.7 Å, are situated in line. The ring centres of the ATP adenosine moieties are shown in green (left image) and cyan (right image) van der Waals spheres (scale factor 0.1).

The docked ATP molecules obtained through two AutoDock Vina trials formed close interactions at separations between 2.8 and 3.5 Å, with residues near the activation loop and active site residues D231 and D249 of HvMAP3K (Figure 5; Supplementary Movies S1 and S2). More precisely, in the first AutoDock Vina trial, ATP interacted with S111, A113, S192, and A235 through H-bonds, and via K233 through electrostatic interactions in the vicinity of the D231 and D249 catalytic residues, where the P_γ phosphate group of ATP is prone to cooperative hydrolysis by nearby D231 (base) and D249 (acid) of HvMAP3K (Figure 5, left panel; Supplementary Movie S1). The ATP molecule, docked through the second AutoDock Vina trial, contacted E122 and E124 (from HvMKK3), Q99, S111, and A113 through H-bonds, and K233 via electrostatic interactions near D231 and D249 catalytic residues of HvMAP3K (Figure 5, right panel; Supplementary Movie S2). We also detected rarely observed interactions of aromatic ring centers of adenosine moieties with amino groups of G114 (HvMAP3K) and K123 (HvMKK3) (Figure 5, van der Waals spheres). Both P_γ groups in HvMAP3K molecules were oriented towards the D231 and D249 catalysts of HvMAP3K, allowing the hydrolysis of ATP at the terminal phosphate group, and were directed towards the P-motif (T245) of HvMKK3. Finally, it was satisfactory to see that the position of the bound ASK1 inhibitor in human MAP3K 5 [52] coincided with that of docked ATP in both AutoDock Vina trials for HvMAP3K.

Based on the HvMAP3K/HvMKK3 complex with docked ATP, it is likely that ATP first diffuses into HvMAP3K and, after hydrolysis by a lytic water molecule through the cooperative action of the catalytic residues, the terminal P_γ group adopts a predicted position at the HvMAP3K/HvMKK3 interface, at distances of 7.8 and 7.9 Å (Figure 5; red dashed lines). This position was also observed in the complex of the HvMKK3 enzyme

with its downstream kinase, HvMAPK [5]. We suggest that during the hydrolysis of ATP in the HvMAP3K/HvMKK3 complex, the flexibility of kinase molecules will change, causing spatial adjustments of residues participating in the phosphorylation process. We acknowledge that during ATP hydrolysis, the flexibility of kinase molecules will cause spatial adjustments of residues that participate in phosphorylation.

2.7. All-Atom Molecular Dynamics (MD) of the HvMAP3K/HvMKK3 Modelled Complex

All-atom MD simulations of the HvMAP3K/HvMKK3 complex were conducted in the OpenMM toolkit [53] for 50 ns in length in three replicates, generating in each case 1001 models clustered in ten medoids (trajectories) (Supplementary Figure S6; Supplementary Movie S3).

The MD data revealed deviations in relative partialities from the dispositions of residues in starting structures and reached the best possible convergence between simulations and consensus protein fluctuations, based on the ff19SB force field in explicit optimal point charge water cube [53] (Supplementary Figure S6A–C). Plotted averaged RMSF values over simulation time (reaching convergence after 30 nanoseconds, based on three replicates) inform protein dynamics and flexibility via trajectories of protein ensembles. The RMSF peak values of catalytic and P-motifs were relatively stable in the HvMAP3K and HvMKK3 molecules (Supplementary Figure S6A–C), although the coil regions separating catalytic residues (respective motifs DNKG and LKGE in HvMAP3K and HvMKK3) were more flexible compared to the loops carrying catalytic residues (Supplementary Figure S6C). Unsurprisingly, the other flexible region in HvMAP3K was the coil region (motif VAK-LATMTAA), which precedes the P-site. Notably, we also observed relatively low mobility of an α-helix in HvMAP3K (motif LFHVGTT, residues 318–324, Supplementary Figure S6C, bottom right), which is located at the interface of the complex. The most flexible region of the complex was positioned at the N-terminus of HvMKK3, while that of HvMAP3K was less mobile. In summary, the MD data of the HvMAP3K/HvMKK3 complex suggested that the flexibility of both protein components was predominantly confined to coil loop regions (Supplementary Figure S6; Supplementary Movie S3).

2.8. Ancestral Sequence Reconstruction of MAP3K Kinases and Latent Space During Evolution

As with the barley HvMKK3 complexed with its downstream substrate HvMAPK enzyme [5], we conducted ancestral sequence reconstruction analyses (ASR) for MAP3K kinases, combined with Variational Autoencoder (VAE) analysis [54], implemented in FireProt^{ASR} v2.0 [55,56]. We applied the default parameter settings for evolutionary models and phylogeny to inform us about the origin of the MAP3K kinase family, specifically regarding the evolution of P-motifs and catalytic machinery (Figures 6 and 7; Supplementary Datasets S2 and S3). This analysis, using the HvMAP3K sequence (UniProt A0A8I7B904; 679 residues) and its closest orthologues, identified 129 ancestors, where the P-motif SMKGT, present in the ancestral root, has evolved into two major lineages with SMKGT and TMKGT motifs. The ancestor sequences contain either the SMKGT motif (Figure 6; magenta rectangles and ovals) or the TMKGT motif (Figure 6; blue rectangles, ovals and italics). Notably, in both lineages, including the ancestral root, the catalytic acid and base residues remained conserved during evolution. Based on these data, we suggest that in the HvMAP3K kinase, the SMKGT P-motif present in the ancestral root evolved into the TMKGT motif present in extant MAP3K sequences through several predecessors.

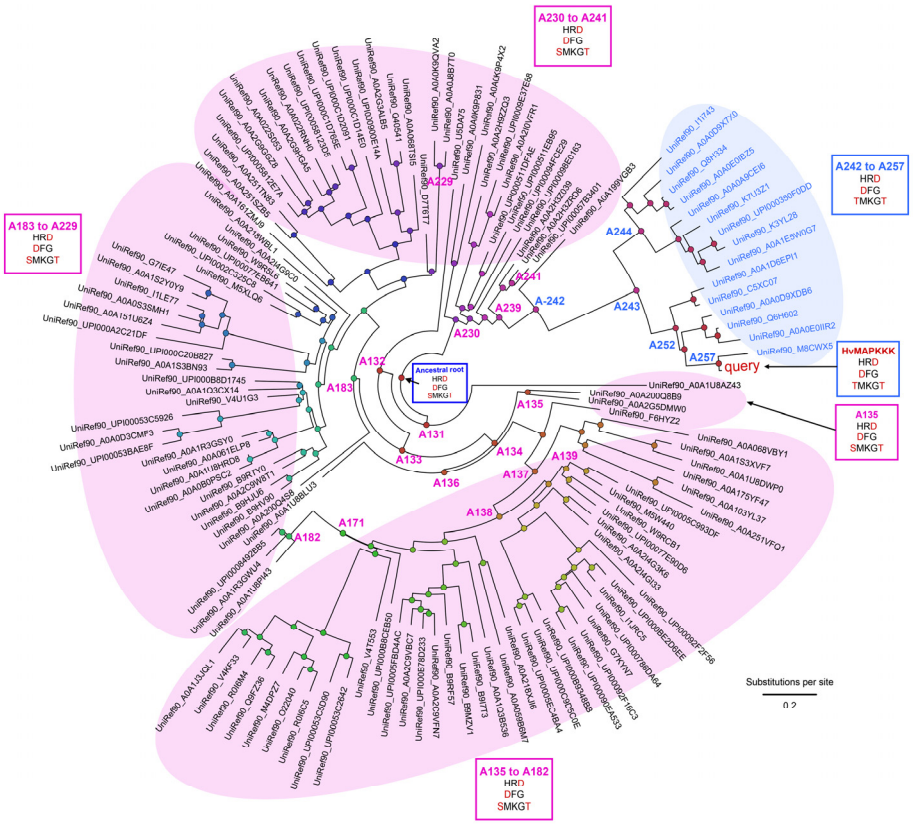

Figure 6. Rooted tree of representative MAP3K enzymes, annotated by NCBI and UniProt accessions (129 in total), with the HvMAP3K sequence indicated in red (UniProt A0A8I7B904). Ancestral sequence reconstruction was conducted using FireProt^{ASR} v2.0 [55,56], conducted with barley MAP3K as input; it identified 129 ancestor sequences with ancestral nodes colour-coded. The ancestral root (dark blue rectangle) carries HRD, DFG, and SMKGT motifs, evolving into two distinct lineages of extant MAP3K enzymes, which contain either the SMKGT motif (magenta rectangles and ovals) or the TMKGT motif (light blue rectangle, oval and letters). Catalytic residues D = base = H^+-acceptor (HRD motif), and D = acid = H^+-donor (DFG motif) remain conserved in both lineages, including the ancestral root. The equivalent residues corresponding to these motifs are indicated for selected ancestral groups. The colouring of node circles in the tree, visualized in FigTree v1.4.4 [57], reflects the order starting from the ancestral root to ancestor 129, shown across the fire/brick-yellow-yellow/green-green-green-cyan-blue-purple hues. Substitutions per site scale are indicated.

Following the ancestral sequence reconstruction of the MAP3K plant family, we recreated its latent space, including the ancestral trajectory, using VAE (Figure 6). Here, we were primarily interested in the conservation of P-motifs and catalytic machinery. The latent space trajectory reconstruction indicated that the TMKGT P-motif in HvMAP3K has evolved through 47 ancestral sequences (ancestors 0–46) from the SMKGT motif present in 54 initial ancestors (ancestors 47–100) (Figure 7, left panel). Notably, of the 149 entries (Figure 7; blue circles in left panel), the monocot MAP3K protein family forms a distinct subset (Figure 7; overlapping blue ovals and entries annotated in blue italics in left panel), compared to the dicot family (Figure 7; annotated in black italics in left panel). The latent trajectory of monocot family enzymes consists of 101 ancestors (Figure 7; ancestor 0 to ancestor 100 shown in overlapping red circles forming a line in the left panel). These SMKGT and TMKGT motifs were carried into the two distinct lineages of plant extant MAP3K sequences. Conversely, in both ancestral groups, including the ancestral root, the catalytic proton acceptor (HRD motif) and proton donor (DFG motif) residues were conserved through evolution in 150 selected sequences (Supplementary Dataset S3). Further analysis of the number of substitutions and insertions/deletions (indels) in the latent space of the

plant MAP3K family indicated that ancestor 101 (Figure 7, cf. left and right panels), which is the least identical progenitor to barley MAP3K or ancestor 0 (50.2% identity between the two sequences), aggregated 262 substitutions (38.6%) and 65 insertions/deletions (9.6%) compared to barley MAP3K (Figure 7, right panel).

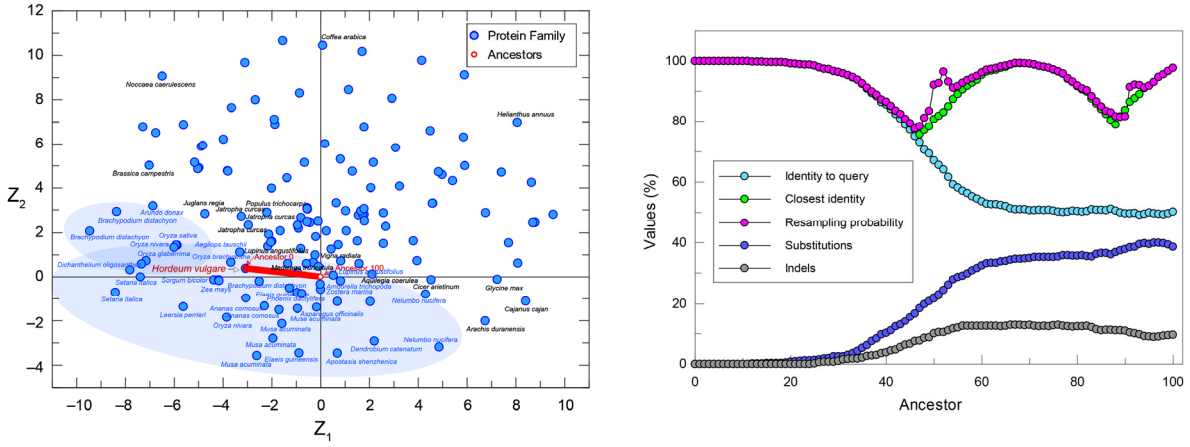

Figure 7. Latent space reconstruction and ancestor trajectory of plant extant MAP3K enzymes. **Left panel**: Latent space reconstruction of the plant MAP3K family is based on barley MAP3K (UniProt A0A8I7B904) and 149 nearest extant plant MAP3K sequences obtained by the UniProt BLAST search, visualized by blue circles. It was conducted using VAE [54] implemented in FireProt^{ASR} v2.0 [55,56]. The monocot MAP3K protein family forms a distinct subset (overlapping blue ovals and entries annotated in blue italics), compared to the dicot family (black italics). The latent trajectory (red line) of 101 ancestors (ancestor 0 to ancestor 100) is shown, with a red circle for each ancestor. The starting point of the trajectory is ancestor 100 (motif SMKGT, from which all ancestral sequences emerge), which evolves through 99 ancestors to ancestor 0 or the MAP3K successor. In the plot, the position of ancestor 0 coincides with that of barley MAP3K, with the TMKGT motif and catalytic residues D231 and D249. **Right panel**: Parameters of ancestors in the latent space of the plant MAP3K family with the following specifications: ancestor 0–100 sequence identities to barley MAP3K (light blue), sequence identity of each ancestor to the closest plant MAP3K (green), resampling probability of the sequence occurrence (magenta), and numbers of substitutions (dark blue) or insertions/deletions (indels; grey) for each ancestor (compared to barley MAP3K).

During docking, there is a combinatorial variation of orientations of MAP3K and MKK kinases that, in principle, defines a 3D space of all possible arrangements of the two proteins interacting. To corroborate this possibility, several MAP3K catalytic modules were taken from the AlphaFold database [58] and superposed with the quaternary structure of the HvMAP3K/HvMKK3 complex (Supplementary Figure S7). This comparison revealed good agreement in RMSD values, secondary structure overlaps and the positions of catalytic residues in the catalytic modules of five plant MAP3K kinases and HvMAP3K.

2.9. Phylogeny of Barley MKK Kinases

To gain an insight into the phylogeny of barley MKK enzymes, a total of 250 sequences homologous to barley MKK3 were retrieved from the UniProt database (Supplementary Dataset S4; pages 1–68). After removing incomplete and duplicate sequences, 231 sequences (Supplementary Dataset S4; pages 68–357) were aligned in ProMals3D [59], where highly similar sequences were pre-aligned without using the consistency scoring function to generate pre-aligned groups. In the next step, one representative sequence, divergent from the others, was selected from each pre-aligned group. In the second step, these 166 representative sequences were aligned progressively according to a consistency scoring function.

These aligned sequences (Supplementary Dataset S4; pages 358–400) were segregated into 78 groups (Supplementary Figure S8) in a rooted tree visualized in FigTree v1.4.4 [57].

We focused predominantly on the analysis of catalytic motifs, including those of ancestral sequences (Supplementary Figure S8, highlighted in green). The search entry of barley MKK3 (UniProt accession A0A140JZ13) contained the conserved HRD/DFG catalytic motif combination (Supplementary Figure S8; blue arrow), while these motifs varied in other barley MKK entries and formed various combinations, such as FRD/DFS, HRD/DFG and HGD/DFS in ancestral sequences, and HRN/DFG, HLE/GFG, HMD/DFG, HLD/DFG, YCD/DFG, HRD/DVG, HGD/DFG, HRD/DFR, HCD/DGF, and YRD/DFG combinations in other MKK entries. Some of these signatures (HRN/DFG and HLE/GFG) appeared to be inconsistent with the catalytic function of kinases, annotated as a protein kinase domain-containing protein and nonfunctional Rpg1, with the respective UniProt accessions A0A8I7BGM1 and Q0Z988.

3. Materials and Methods

3.1. Computational Methods

The catalytic domain of HvMAP3K, 270 residues was constructed using the SWISS-MODEL server (Biocentrum, Basel, Switzerland) [60] and the crystal structure of the human MAP3K 5 kinase (PDB accession 5UOX, chain A) [52], as a template, at 43.5% sequence identity between the two sequences. The human MAP3K 5 kinase also contains a bound ASK1 (Apoptosis Signal-regulating Kinase 1) inhibitor [52]. The 35-residue C-terminal component of the HvMAP3K catalytic domain was excluded from modelling, as it forms a flexible loop. The theoretical 3D model of the full-length HvMKK3 enzyme was retrieved from the AlphaFold Protein Structure Database (accession A0A140JZ13) [58,61]. The full-length sequences and accession numbers of HvMAP3K and HvMKK3 are specified (Supplementary Figure S1). The coordinates of the 3D model of the catalytic domain of HvMAP3K are available in the ModelArchive repository (https://modelarchive.org/), under the accession code ma-iprgc.

The quaternary model of the HvMAP3K/HvMKK3 complex was calculated via HDOCK (Huazhong University of Science and Technology, Wuhan, China), which employs a hybrid algorithm of template-based modeling and ab initio free docking of protein–protein and protein–ligand systems to generate docking poses for each model [45]. The top HvMAP3K/HvMKK3 model complex was selected from 100 models based on the criteria specified in Section 2.5. (dispositions of P-motifs; orientations of N- and C-termini, interface interactions). The MAP3K molecule of the top selected complex was rotated towards the HvMKK3 molecule to improve structural compactness and binding energy between the two kinases, predicted by the Protein Binding Affinity Predictor for Multiple Complexes (PPAP) tool [46]. The resultant top-scoring complex was energy-minimized using the knowledge-based Yasara2 force field (bond distances, planarity of peptide bonds, bond angles, Coulomb terms, dihedral angles, van der Waals forces) [62] combined with the particle-mesh-Ewald energy function for long-range electrostatics at a cut-off of 8.0 Å to obtain smooth electrostatic potentials [63]. Distorted covalent geometry and conformational stress were removed by short steepest descent minimization (time 5000 fs, 1 ft time steps, 298 K), followed by simulated annealing with 1 fs time steps, atom velocities scaled down by 0.9 every 10th step, until convergence at 710 steps with energy improvement of >0.05 kJ/mol per atom during 200 steps. The quality of geometrical and stereochemical parameters of the HvMAP3K/HvMKK3 complex, consisting of 793 residues, was evaluated by the Ramachandran plot analysis [64,65]. There were no violations of stereochemical parameters in the minimized complex, except Y312, which was also violated in the model of HvMAP3K (constructed via the SWISS-MODEL server) and K180 of HvMKK3 taken from

the AlphaFold Protein Structure Database. Both residues were positioned on loops distant from the catalytic machinery and P-sites of both kinases, thus without direct effects on the interactions of the HvMAP3K and HvMKK3 kinases in the complex. The coordinates of the quaternary model of the HvMAP3K/HvMKK3 complex are available in the ModelArchive repository (https://modelarchive.org/), under the accession code ma-jre4o.

To examine the precise dispositions of ATP molecules in cavities shared by both molecules in the HvMAP3K/HvMKK3 complex, we used AutoDock Vina v1.2.7 (The Scripps Research Institute, CA, USA) [50]. Employing this docking technique, we selected a target rectangular box of approximately 12 × 12 × 15 Å in the vicinity of the catalytic residues of the HvMAP3K complex at the interface of both kinases. The ATP molecule was docked with H-atoms and merged charges, with no ion pairs in the complex, while these selections were ignored for the ATP molecule. Docking produced ten ATP poses, which were scored by binding affinities (kcal/mol) and dispositions of $P_{\alpha,\beta,\gamma}$ phosphate groups relative to the HvMAP3K catalytic residues. This score aggregates electrostatic, van der Waals, and conformational factors, allowing ranking of ligand poses [50].

All-atom MD simulations of the HvMAP3K/HvMKK3 complex (12,401 atoms including hydrogens, 213 Na^+ and Cl^- ions, and 28,735 water molecules, for a total of 98,819 atoms) were conducted using the OpenMM toolkit v2008-2025 (Stanford University, CA, USA) as implemented in Tamarind Bio (San Francisco, CA, USA) [46]. We executed these simulations in three replicates within a van der Waals box of 100.86 × 114.40 × 102.44 Å (x-y-z dimensions) and a volume of 1,182,040.46 $Å^3$, containing a fully solvated protein complex. We used the following specifications for MD simulations: maximal minimization steps (10,000), equilibration time (0.2 ns), production time (50 ns), force field (ff19SB), integration step size (0.2), box padding (12 Å), ion concentrations (Na^+, Cl^-, 0.15 M), temperature (298 K), pressure (1 bar), starting force constant (1.00 kcal/mole per $Å^2$), equilibration trajectory frequency (1000 steps), and production trajectory frequency (1000 steps). We determined root mean square fluctuation (RMSF) values (measures of the displacement of the Cα atoms relative to those of a starting structure) based on the initial input structures (presented as averaged RMSF values in Supplementary Figure S6A) and the convergence and radius of gyration values for the three 50 ns replicates (Supplementary Figure S6B). These MD simulations produced 1001 3D models in each replicate that we clustered into 10 medoids (trajectories) (Supplementary Figure S6C, Supplementary Movie S3).

3.2. Identification of Phosphorylation Sites of HvMAP3K

The P-motifs in HvMKK3 and HvMAP3K were identified with MusiteDeep [44]. The consensus phosphorylation sites on serine, threonine, and tyrosine (Tyr) residues (which occur in less than 1% of cases on Tyr residues) were predicted, together with those containing consensus motifs with a high likelihood of being phosphorylated. The MusiteDeep prediction data were confirmed with the NetPhos3.1 analysis (accessed 26 January 2026) [44].

3.3. Identification of Cavities in the HvMAP3K/HvMKK3 Complex

Cavities in the HvMAP3K/HvMKK3 complex were evaluated using the DoGSiteScorer tool [66] implemented in ProteinsPlus [67]. DoGSiteScorer is a grid-based method that uses a difference of Gaussian filter to detect potential binding pockets, solely based on the 3D structure of a protein. It splits the structure into sub-pockets, for which it calculates global properties, describing their volume, surface, shape, and chemical features.

3.4. Structural Analysis of HvMAP3K by InterPro

Protein structural analysis was conducted using the InterPro tool (accessed 28 January 2026), which is based on the classification of the Protein Database Consortium, and integrates several databases (referred to as member databases) [47]. This tool, which provides annotations for over 200 million protein sequences, generates predictive protein models according to their signatures and classifies them into families.

3.5. Ancestral Sequence Reconstruction (ASR) Phylogeny of the MAP3K Protein Family and Its Latent Evolutionary Space Trajectory Reconstruction

A phylogenetic tree of HvMAP3K entries containing ancestor and successor sequences was generated using FireProt^{ASR} v2.0 [55,56] (accessed 30 January 2026) and visualized in FigTree v1.4.4 [57], as described previously [5,68,69]. We first searched the UniProt database, using its Basic Local Alignment Search Tool v2.17.0 (BLAST) [70] with the full-length HvMAP3K sequence (UniProt A0A8I7B904; 679 residues) and identified 250 closely related plant sequences. In the next step, we conducted automated ASR using default parameter settings for evolutionary models and phylogeny (bootstraps 50, gap correction 0.5, clustering identity filter 0.9 at 30–80% sequence identity to HvMAP3K) to identify ancestral and successor sequences. After homology search and filtering, this step aggregated the dataset of 358 sequences homologous to HvMAP3K, specifying 129 ancestral and 129 successor sequences (Supplementary Dataset S2), which allowed the construction of a rooted phylogenetic tree. The tree, drawn to scale, contains ancestors and successors; successors are annotated with National Centre for Biotechnology Information (NCBI) or UniProt accession numbers. Evolutionary distances were computed using the p-distance method and are expressed in units of residue number difference per site.

Latent space trajectory reconstruction of plant extant MAP3K enzymes, using VAE, was calculated in FireProt^{ASR} v2.0 [54–56] (accessed 31 January 2026). We first searched with barley MAP3K (UniProt A0A8I7B904) and the following settings (HvMAP3K selected evolutionary query, multiple sequence alignment at the clustering of 90%; reconstruction of 101 ancestors through dynamic decay) and obtained 249 closest extant plant MAP3K sequences using the Basic Local Alignment Search Tool (BLAST) in the UniProt database [16]. This analysis generated the latent space and ancestral trajectory for the plant MAP3K family, consisting of 150 input sequences and 101 ancestors (numbered as ancestor 0 to ancestor 100) (Supplementary Dataset S3), visualized by red circles as a trajectory along the positions of 150 input successors. We also provide parameters for ancestors in the latent space of the plant MAP3K family, such as a sequence identity of each ancestor to barley MAP3K, the closest sequence identity of each ancestor to the corresponding plant MAP3K, a resampling probability of sequence occurrence in latent space, and the numbers of substitutions and insertions/deletions (indels) for each ancestor (compared to barley MAP3K).

3.6. Phylogenetic Analysis of Barley MKK Kinases

A total of 250 barley sequences homologous to barley MKK3 were retrieved from the UniProt database, from which incomplete and duplicate sequences were removed (Supplementary Dataset S4). From 231 sequences, 166 sequences (annotated by UniProt numbers) were used in ProMals3D [59] to generate 78 pre-aligned groups. The following alignment parameters were used: identity threshold above which fast alignment is applied: 0.6; weight for constraints derived from sequences: 1; weight for constraints derived from homologs with structures: 1.5; weight for constraints derived from input structures: 1.5; weight for amino acid residue scores: 0.8; weight for predicted secondary structure scores: 0.2; parameters for aligning sequences within groups in the first alignment stage: align sequences by mafft. Catalytic motifs of all entries, corresponding to the conserved HRD

and DFG motifs present in barley MKK3 (UniProt accession A0A140JZ13), were inspected. The tree was visualized in FigTree v1.4.4 [57] (accessed 1 February 2026).

3.7. Copy Number of the HvMKK3 Gene in Barley Pan-Genome Cultivars

A total of 76 Barley pan-genome (BPGv2) cultivar/accession assemblies [9,17] were analyzed for copy numbers of the *MAP3K* gene (UniProt accession A0A8I7B904) at the Leibniz Institute of Plant Genetics and Crop Plant Research (Gatersleben, Germany; https://panbarlex.ipk-gatersleben.de; accessed 24 June 2026).

4. Conclusions

In the in silico experiments described above, we have used computational methods combined with phylogeny and mechanistic assessments to generate a quaternary protein structure of the catalytic domain of the barley HvMAP3K kinase with the downstream full-length HvMKK3 enzyme, working as a functional unit. The MAPK cascade enzymes transmit regulatory and external environmental signals to the nucleus, where gene transcriptional patterns are altered accordingly. These biological processes are specified under the GO:0000165 category in the Gene Ontology Resource 6 (https://geneontology.org; accessed 24 June 2026) [71]. It is clear that combinations (hubs) of interacting MAP kinase cascade enzyme isoforms are numerous, highly diversified and largely undefined [72]. However, in our recent studies, we have characterized the interactions of the specific barley MAP3K, *MKK3* and MAPK isoenzymes that constitute at least part of the MAPK cascade involved in the dormancy to germination transition (Figure 1).

More specifically, through molecular modelling and docking, we have determined the disposition of the catalytic domain of the barley MAP3K enzyme (270 residues) in complex with barley MKK3 (523 residues). The defined structure of the MAP3K domain is flanked by a disordered N-IDR of 95 residues and a C-IDR of 277 residues. Both IDRs contain flexible segments, which is consistent with their unstructured nature; these IDRs contain protein sequence motifs implicated in binding regulatory molecules in other MAPK enzymes. The barley MAP3K/MKK3 complex is stabilised by electrostatic surface potentials formed by the residues and their neighbours positioned at the interface of the protein complex.

Based on the theoretical quaternary model of HvMAP3K/HvMKK3 with bound ATP, we identified the HRD/DFG catalytic motif of HvMAP3K that is cooperatively involved in ATP hydrolysis, together with the prospective projection of a released phosphoryl group through the enzyme to its target phosphorylation site at the activation loop of HvMKK3. The presence of Thr phosphorylation sites in the HvMAP3K enzyme (motif TMKGT) raises the possibility that an unknown upstream kinase could phosphorylate and activate the MAP3K enzyme; an alternative possibility is that MAP3K undergoes autophosphorylation.

A single copy of the *MAP3K* gene is located on barley chromosome 5H in 76 pan-genome assemblies. The conservation of a single copy of the *MAP3K* gene and the high level of protein sequence identity across the pan-genome assemblies may be compared with the downstream *MKK3* gene, which in domesticated barley accessions can contain several tandemly arranged gene copies and several genetic variants that influence *MKK3* activity [4].

Although no enzymatic activity data for HvMAP3K are available, the previous observation that higher levels of HvMKK3 activity shorten dormancy and promote germination suggests that increases in HvMAP3K activity would also increase MKK3 activity and thereby shorten dormancy. Thus, if the activity of the MAP3K enzyme were blocked, dormancy would be extended. Alternatively, if any putative inactivation of MAP3K were released, the dormancy to germination transition could proceed.

5. Future Directions

Although our data and conclusions on the MAP3K to MKK3 and the MAPK3 to MAPK reactions are consistent with well-documented experimental data from other plant MAPK systems (Figure 1), the modelling data presented here must nevertheless be validated through future genetic, biochemical, and experimental structural biology approaches [5].

Additional upstream kinases, the identity of the mitogen receptors involved in dormancy and germination, and transcription factors that modulate appropriate changes in gene expression have not yet been defined. Central aims of future research will be focused on these factors. Our strategy here was to walk one step upstream from MKK3 to MAP3K. This approach could be continued step-by-step upstream to the mitogen and step-by-step downstream from HvMAPK to the transcription factor and the genes it transcribes, all of which are likely to necessitate co-expression and associated network analyses [73]. Mutant libraries and targeted mutagenesis will be important for the generation and testing of candidate genes [74].

Data from the present study identify additional gaps in our knowledge of the dormancy to germination transition in barley, including the experimental confirmation of potential roles for several sequence motifs in MAP3K IDRs that have been implicated elsewhere as binding sites for regulators that mediate enzymatic action, specificity and turnover. Gene silencing technologies could be applied to confirm the potential molecular and biological functions of these motifs; the mutated lines could be tested for dormancy/germination as described by Jørgensen et al. [4]. An additional challenging goal to define the structures of IDRs and disordered-to-ordered reactions could be approached using cryogenic electron tomography, nuclear magnetic resonance and circular dichroism spectroscopy, paramagnetic relaxation enhancement integrated with molecular dynamics simulations, machine learning, and protein engineering [75].

It would seem sensible at this stage to focus on defining the precise genetics, structural biology and biochemistry of ABA action both in maintaining dormancy and pausing germination when deteriorating environmental conditions threaten the viability of the young seedling. Identification of the activating mitogen of ABA action would be a highly important experimental target, as recently reported for the role of the fungal effector HCE1 that regulates the plant immune response in Arabidopsis [76].

However, if we are to completely define the MAPK cascade enzyme complexes in precise biophysical terms, there are elementary but challenging tasks to achieve. Identifying in vivo interacting partners of the cascade could involve yeast two-hybrid techniques, gene co-expression studies, and biochemical approaches such as fluorescence (or Förster) resonance energy transfer assays, affinity chromatography, co-immunoprecipitation or proximity labelling. Defining 3D structures of the MAPK cascade enzymes and their binary complexes by X-ray crystallography [76] and cryogenic electron microscopy at high resolution [77] would confirm the structural modelling described here, as would quantifying thermodynamic parameters of binding of the MAPK cascade enzyme binary complexes and the roles of binding residues through biophysical techniques of isothermal titration calorimetry, surface plasmon resonance or nuclear magnetic resonance titrations in wild-type and mutant kinases.

Supplementary Materials: The following supporting information can be downloaded at https://www.mdpi.com/article/10.3390/kinasesphosphatases4040030/s1. Supplementary Figure S1. Protein sequences of barley MAP3K NPK1-like (HvMAP3K) and *MKK3* (HvMKK3) kinases, and their GenBank, Swiss-Model Depository, AlphaFold Structure Database and UniProt (when applicable) accessions. Supplementary Figure S2. Genetics of the barley *MAP3K* gene. Supplementary Figure S3. Multiple sequence alignment using Clustal Omega v1.2.4 of plant MAP3K kinases annotated by UniProt or GenBank accession numbers. Supplementary Figure S4. Stereo representation of the

HvMAP3K/HvMKK3 model complexes illustrates the top-ranked complex and two additional complexes with unfavourably docked HvMKK3. Supplementary Figure S5. The HvMAP3K/HvMKK3 complex and its internal cavities. Supplementary Figure S6. Full-atom MD simulations of the HvMAP3K/HvMKK3 complex, using the OpenMM toolkit (cf. Supplementary Movie S3). Supplementary Figure S7. Superposition of the HvMAP3K (blue)/HvMKK3 (pink) complex and catalytic modules of four plant kinases (grey). Supplementary Figure S8. Phylogenetic tree of barley MKK kinases homologous to barley *MKK3* and catalytic motifs. Supplementary Movie S1. Animations of the HvMAP3K/HvMKK3 complex with docked ATP (cf. Figure 5, left panel). Supplementary Movie S2. Animations of the HvMAP3K/HvMKK3 complex with docked ATP (cf. Figure 5, right panel). Supplementary Movie S3. Animations of the MD trajectory of the HvMAP3K/HvMKK3 complex (cf. Supplementary Figure S6). Supplementary Movies 1–3 are available in the Figshare repository under 34845960 (https://doi.org/10.6084/m9.figshare.34845960). Supplementary Dataset S1. Global alignment of 76 haplotypes. Supplementary Dataset S2. Figure 6. 129 Aligned ancestors; Figure 6. 129 Aligned successors; Figure 6. 150 Input sequences. Supplementary Dataset S3. Figure 7. 150 Input listed sequences; Figure 7. 101 Aligned ancestors. Supplementary Dataset S4. Supplementary Figure S8. 250 Listed sequences; Supplementary Figure S8. 231 Aligned sequences in ProMals3D; Supplementary Figure S8. 166 Listed sequences.

Author Contributions: Conceptualization M.H. and G.B.F.; data curation M.H. and J.G.S.; investigation M.H. and J.G.S.; formal analysis M.H. and G.B.F.; visualization M.H. and J.G.S.; writing—original draft M.H. and G.B.F.; writing—review and editing M.H. and G.B.F. All authors have read and agreed to the published version of the manuscript.

Funding: This work was supported by the Australian Research Council (grant DP120100900 to M.H.). M.H. was supported by Adelaide University and the Waite Research Institute. Plant SynBio Australia is made possible through investment funding provided by the Commonwealth Government National Collaborative Research Infrastructure Strategy (NCRIS).

Institutional Review Board Statement: Not applicable.

Informed Consent Statement: Not applicable.

Data Availability Statement: The data presented in this study are available upon request from the corresponding author.

Acknowledgments: We thank Birgitte Skadhauge and Christoph Docktor (Carlsberg Research Laboratory, Copenhagen V, Denmark) for their long-term support of our collaboration (B.S.) and comments on the draft manuscript (C.D.), and Nils Stein (Leibniz Institute of Plant Genetics and Crop Plant Research) for providing the barley pan-genome data before publication. We acknowledge the contribution from Ira Wight (Tamarind Bio, Stanford University, CA, USA).

Conflicts of Interest: The authors declare no conflicts of interest.

Abbreviations

ABA, abscisic acid; AI, artificial intelligence; ASK1, Apoptosis Signal-regulating Kinase 1; BLAST, basic local alignment search tool; CPK, Corey-Pauling-Koltun; H-bond, hydrogen bond; kTe^{-1}, units of electrostatic surface potentials, where k = Boltzmann constant, T = absolute temperature per electron; IDR(s), intrinsically disordered region(s); K_D; affinity binding constant; *MKK3* (MAP2K), mitogen-activated protein kinase kinase 3; MAPK, mitogen-activated protein kinase; MAPKK, mitogen-activated protein kinase kinase; MAPKKK, MAP3K or MEKK, mitogen-activated protein kinase kinase kinase; MAP4K, mitogen-activated protein kinase kinase kinase kinase; MD, molecular dynamics; NCBI, National Centre for Biotechnology Information; lDDT, Local Distance Difference Test; PP2C, C2 Protein Phosphatase; P-motif, phosphorylation motif; PPAP, Protein Binding Affinity Predictor for Multiple Complexes; QTL, quantitative trait locus; RMSD, root mean square deviation; RMSF, root mean square fluctuation; VAE, Variational Autoencoder; VCL, VideoLAN Client.

References

1. Zhang, M.; Zhang, S. Mitogen-activated protein kinase cascades in plant signaling. *J. Integr. Plant Biol.* **2022**, *64*, 301–341. [CrossRef]
2. Li, R.; Hameed, M.U.; Geuten, K. Translating research on seed dormancy and germination from Arabidopsis to temperate cereals to control pre-harvest sprouting. *Front. Plant Sci.* **2026**, *17*, 1763984. [CrossRef]
3. Li, Y.; Li, Y.; Zou, X.; Jiang, S.; Cao, M.; Chen, F.; Yin, Y.; Xiao, W.; Liu, S.; Guo, X. Bioinformatic identification and expression analyses of the MAPK–MAP4K gene family reveal a putative functional MAP4K10-MAP3K7/8-MAP2K1/11-MAPK3/6 cascade in wheat (*Triticum aestivum* L.). *Plants* **2024**, *13*, 941. [CrossRef]
4. Jørgensen, M.T.; Vequaud, D.; Wang, Y.; Andersen, C.B.; Bayer, M.; Box, A.; Braune, K.B.; Cai, Y.; Chen, F.; Cuesta-Seijo, J.A. Post-domestication selection of MKK3 shaped seed dormancy and end-use traits in barley. *Science* **2026**, *391*, 90–95. [CrossRef]
5. Hrmova, M.; Dockter, C.; Krsticevic, F.; Jørgensen, M.E.; Skadhauge, B.; Fincher, G.B. Dormancy versus germination: 3D Protein modeling and evolutionary analyses define the roles of genetic variants in the barley MKK3 enzyme. *Int. J. Mol. Sci.* **2026**, *27*, 530. [CrossRef]
6. Wang, Z.; Gou, X. Receptor-like protein kinases function upstream of MAPKs in regulating plant development. *Int. J. Mol. Sci.* **2020**, *21*, 7638. [CrossRef]
7. Neupane, A.; Nepal, M.P.; Piya, S.; Subramanian, S.; Rohila, J.S.; Reese, R.N.; Benson, B.V. Identification, nomenclature, and evolutionary relationships of mitogen-activated protein kinase (MAPK) genes in soybean. *Evol. Bioinform.* **2013**, *9*, EBO-S12526. [CrossRef]
8. Cui, L.; Yang, G.; Yan, J.; Pan, Y.; Nie, X. Genome-wide identification, expression profiles and regulatory network of MAPK cascade gene family in barley. *BMC Genom.* **2019**, *20*, 750. [CrossRef]
9. Jayakodi, M.; Lu, Q.; Pidon, H.; Rabanus-Wallace, M.T.; Bayer, M.; Lux, T.; Guo, Y.; Jaegle, B.; Badea, A.; Bekele, W.; et al. Structural variation in the pangenome of wild and domesticated barley. *Nature* **2024**, *636*, 654–662. [CrossRef]
10. Zhan, H.; Yue, H.; Zhao, X.; Wang, M.; Song, W.; Nie, X. Genome-wide identification and analysis of MAPK and MAPKK gene families in bread wheat (*Triticum aestivum* L.). *Genes* **2017**, *8*, 284. [CrossRef]
11. Pan, L.; De Smet, I. Expanding the Mitogen-Activated Protein Kinase (MAPK) Universe: An Update on MAP4Ks. *Front. Plant Sci.* **2020**, *11*, 1220. [CrossRef]
12. Ichimura, K.; Shinozaki, K.; Tena, G.; Sheen, J.; Henry, Y.; Champion, A.; Kreis, M.; Zhang, S.; Hirt, H.; Wilson, C.; et al. Mitogen-activated protein kinase cascades in plants: A new nomenclature. *Trends Plant Sci.* **2002**, *7*, 301–308. [CrossRef]
13. Danquah, A.; de Zélicourt, A.; Boudsocq, M.; Neubauer, J.; Frei Dit Frey, N.; Leonhardt, N.; Pateyron, S.; Gwinner, F.; Tamby, J.-P.; Ortiz-Masia, D.; et al. Identification and characterization of an ABA-activated MAP kinase cascade in Arabidopsis thaliana. *Plant J.* **2015**, *82*, 232–244. [CrossRef]
14. Matsuoka, D.; Yasufuku, T.; Furuya, T.; Nanmori, T. An abscisic acid inducible Arabidopsis MAPKKK, MAPKKK18 regulates leaf senescence via its kinase activity. *Plant Mol. Biol.* **2015**, *87*, 565–575. [CrossRef]
15. Jin, H.; Axtell, M.J.; Dahlbeck, D.; Ekwenna, O.; Zhang, S.; Staskawicz, B.; Baker, B. NPK1, an MEKK1-like mitogen-activated protein kinase kinase kinase, regulates innate immunity and development in plants. *Dev. Cell* **2002**, *3*, 291–297. [CrossRef]
16. Ahmad, S.; Jose da Costa Gonzales, L.; Bowler-Barnett, E.H.; Rice, D.L.; Kim, M.; Wijerathne, S.; Luciani, A.; Kandasaamy, S.; Luo, J.; Watkins, X.; et al. UniProt Consortium. The UniProt website API: Facilitating programmatic access to protein knowledge. *Nucleic Acids Res.* **2025**, *53*, W547–W553. [CrossRef]
17. Jayakodi, M.; Padmarasu, S.; Haberer, G.; Bonthala, V.S.; Gundlach, H.; Monat, C.; Lux, T.; Kamal, N.; Lang, D.; Himmelbach, A. The barley pan-genome reveals the hidden legacy of mutation breeding. *Nature* **2020**, *588*, 284–289. [CrossRef]
18. Nakamura, S.; Pourkheirandish, M.; Morishige, H.; Kubo, Y.; Nakamura, M.; Ichimura, K.; Seo, S.; Kanamori, H.; Wu, J.; Ando, T.; et al. Mitogen-activated protein kinase kinase 3 regulates seed dormancy in barley. *Curr. Biol.* **2016**, *26*, 775–781. [CrossRef]
19. Mascher, M.; Jayakodi, M.; Shim, H.; Stein, N. Promises and challenges of crop translational genomics. *Nature* **2024**, *636*, 585–593. [CrossRef]
20. Wonneberger, R.; Schreiber, M.; Haaning, A.; Muehlbauer, G.J.; Waugh, R.; Stein, N. Major chromosome 5H haplotype switch structures the European two-rowed spring barley germplasm of the past 190 years. *Theor. Appl. Genet.* **2023**, *136*, 174. [CrossRef]
21. Li, Z.; Defoort, J.; Tasdighian, S.; Maere, S.; Van de Peer, Y.; De Smet, R. Gene duplicability of core genes is highly consistent across all angiosperms. *Plant Cell* **2016**, *28*, 326–344. [CrossRef]
22. Ginell, G.M.; Emenecker, R.J.; Lotthammer, J.M.; Keeley, A.T.; Plassmeyer, S.P.; Razo, N.; Usher, E.T.; Pelham, J.F.; Holehouse, A.S. Sequence-based prediction of intermolecular interactions driven by disordered regions. *Science* **2025**, *388*, eadq8381. [CrossRef]
23. Sun, X.; Rikkerink, E.H.; Jones, W.T.; Uversky, V.N. Multifarious roles of intrinsic disorder in proteins illustrate its broad impact on plant biology. *Plant Cell* **2013**, *25*, 38–55. [CrossRef]
24. Lobo, S.; Griem, L.; Shell, M.S.; Shea, J.E. amyloid-predict and LLPS-predict: Predicting phase separation propensities in the intrinsically disordered proteome. *Proc. Natl. Acad. Sci. USA* **2026**, *123*, e2531932123. Erratum in: *Proc. Natl. Acad. Sci. USA* **2026** *123*, e2631666123. [CrossRef]

25. Ma, Y.; Yang, L.; Chen, Y.; Chen, M.W.; Yu, W.; Dai, Y. Directed evolution of functional intrinsically disordered proteins. *Nat. Chem. Biol.* **2026**, *22*, 1469–1478. [CrossRef]
26. Jiang, M.; Zhang, Y.; Li, P.; Jian, J.; Zhao, C.; Wen, G. Mitogen-activated protein kinase and substrate identification in plant growth and development. *Int. J. Mol. Sci.* **2022**, *23*, 2744. [CrossRef]
27. Sharrocks, A.D.; Yang, S.H.; Galanis, A. Docking domains and substrate-specificity determination for MAP kinases. *Trends Biochem. Sci.* **2000**, *25*, 448–453. [CrossRef]
28. Bardwell, L.; Shah, K. Analysis of mitogen-activated protein kinase activation and interactions with regulators and substrates. *Methods* **2006**, *40*, 213–223. [CrossRef]
29. Akella, R.; Moon, T.M.; Goldsmith, E.J. Unique MAP Kinase binding sites. *Biochim. Biophys. Acta* **2008**, *1784*, 48–55. [CrossRef]
30. Zeke, A.; Bastys, T.; Alexa, A.; Garai, Á.; Mészáros, B.; Kirsch, K.; Dosztányi, Z.; Kalinina, O.V.; Reményi, A. Systematic discovery of linear binding motifs targeting an ancient protein interaction surface on MAP kinases. *Mol. Syst. Biol.* **2015**, *11*, 837. [CrossRef]
31. Garai, Á.; Zeke, A.; Gógl, G.; Törő, I.; Fördős, F.; Blankenburg, H.; Bárkai, T.; Varga, J.; Alexa, A.; Emig, D.; et al. Specificity of linear motifs that bind to a common mitogen-activated protein kinase docking groove. *Sci. Sig.* **2012**, *5*, ra74. [CrossRef]
32. Mariani, V.; Biasini, M.; Barbato, A.; Schwede, T. lDDT: A local superposition-free score for comparing protein structures and models using distance difference tests. *Bioinformatics* **2013**, *29*, 2722–2728. [CrossRef]
33. Das, A.K.; Helps, N.R.; Cohen, P.T.; Barford, D. Crystal structure of the protein serine/threonine phosphatase 2C at 2.0 A resolution. *EMBO J.* **1996**, *15*, 6798–6809. [CrossRef]
34. Schweighofer, A.; Kazanaviciute, V.; Scheikl, E.; Teige, M.; Doczi, R.; Hirt, H.; Schwanninger, M.; Kant, M.; Schuurink, R.; Mauch, F.; et al. The PP2C-type phosphatase AP2C1, which negatively regulates MPK4 and MPK6, modulates innate immunity, jasmonic acid, and ethylene levels in Arabidopsis. *Plant Cell* **2007**, *19*, 2213–2224. [CrossRef]
35. Soon, F.F.; Ng, L.M.; Zhou, X.E.; West, G.M.; Kovach, A.; Tan, M.H.; Suino-Powell, K.M.; He, Y.; Xu, Y.; Chalmers, M.J.; et al. Molecular mimicry regulates ABA signaling by SnRK2 kinases and PP2C phosphatases. *Science* **2012**, *33*, 85–88. [CrossRef]
36. Ghanizadeh, H.; Qamer, Z.; Zhang, Y.; Wang, A. The multifaceted roles of PP2C phosphatases in plant growth, signaling, and response to abiotic and biotic stress. *Plant Commun.* **2025**, *6*, 101457. [CrossRef]
37. Miyazono, K.; Miyakawa, T.; Sawano, Y.; Kubota, K.; Kang, H.J.; Asano, A.; Miyauchi, Y.; Takahashi, M.; Zhi, Y.; Fujita, Y.; et al. Structural basis of abscisic acid signalling. *Nature* **2009**, *462*, 609–614. [CrossRef]
38. Vish, K.J.; Huet-Calderwood, C.; Ha, B.H.; Calderwood, D.A.; Boggon, T.J. Structural basis for MEKK2 dimerization and substrate recognition. *Nat. Commun.* **2025**, *17*, 193. [CrossRef]
39. Beenstock, J.; Mooshayef, N.; Engelberg, D. How do protein kinases take a selfie (autophosphorylate)? *Trends Biochem. Sci.* **2016**, *41*, 938–953. [CrossRef]
40. Godderz, D.; Schafer, E.; Palanimurugan, R.; Dohmen, R.J. The N-terminal unstructured domain of yeast ODC functions as a transplantable and replaceable ubiquitin-independent degron. *J. Mol. Biol.* **2011**, *407*, 354–367. [CrossRef]
41. Arkinson, C.; Dong, K.C.; Gee, C.L.; Martin, A. Mechanisms and regulation of substrate degradation by the 26S proteasome. *Nat. Rev. Mol. Cell Biol.* **2025**, *26*, 104–222. [CrossRef]
42. Sun, H.L.; Wang, X.J.; Ding, W.H.; Zhu, S.Y.; Zhao, R.; Zhang, Y.X.; Xin, Q.; Wang, X.F.; Zhang, D.P. Identification of an important site for function of the type 2C protein phosphatase ABI2 in abscisic acid signalling in Arabidopsis. *J. Exp. Bot.* **2011**, *62*, 5713–5725. [CrossRef]
43. Wang, D.; Zeng, S.; Xu, C.; Qiu, W.; Liang, Y.; Joshi, T.; Xu, D. MusiteDeep: A deep-learning framework for general and kinase-specific phosphorylation site prediction. *Bioinformatics* **2017**, *33*, 3909–3916. [CrossRef]
44. Blom, N.; Sicheritz-Pontén, T.; Gupta, R.; Gammeltoft, S.; Brunak, S. Prediction of post-translational glycosylation and phosphorylation of proteins from the amino acid sequence. *Proteomics* **2004**, *4*, 1633–1649. [CrossRef]
45. Yan, Y.; Tao, H.; He, J.; Huang, S.Y. The HDOCK server for integrated protein–protein docking. *Nat. Protoc.* **2020**, *15*, 1829–1852. [CrossRef]
46. Tamarind Bio. State of the Art Computational Tools for Biology. Available online: https://www.tamarind.bio/ (accessed on 22 September 2026).
47. Blum, M.; Andreeva, A.; Florentino, L.C.; Chuguransky, S.R.; Grego, T.; Hobbs, E.; Pinto, B.L.; Orr, A.; Paysan-Lafosse, T.; Ponamareva, I.; et al. InterPro: The protein sequence classification resource in 2025. *Nucleic Acids Res.* **2025**, *53*, D444–D456. [CrossRef]
48. Söding, J.; Biegert, A.; Lupas, A.N. The HHpred interactive server for protein homology detection and structure prediction. *Nucleic Acids Res.* **2005**, *3*, W244–W248. [CrossRef]
49. Berman, H.M.; Henrick, K.; Nakamura, H. Announcing the worldwide Protein Data Bank. *Nat. Struct. Biol.* **2003**, *10*, 980. [CrossRef]
50. Eberhardt, J.; Santos-Martins, D.; Tillack, A.F.l.; Forli, S. AutoDock Vina 1.2.0: New Docking Methods, Expanded Force Field, and Python Bindings. *J. Chem. Inf. Mod.* **2021**, *61*, 3891–3898. [CrossRef]

51. Pires, D.E.; Ascher, D.B. CSM-lig: A web server for assessing and comparing protein-small molecule affinities. *Nucleic Acids Res.* **2016**, *44*, W557–W561. [CrossRef]
52. Lanier, M.; Pickens, J.; Bigi, S.V.; Bradshaw-Pierce, E.; Chambers, A.; Cheruvallath, Z.S.; Cole, D.; Dougan, D.R.; Ermolieff, J.; Gibson, T. Structure-based design of ASK1 inhibitors as potential agents for heart failure. *ACS Med. Chem. Lett.* **2017**, *8*, 316–320. Erratum in: *ACS Med. Chem. Lett.* **2017** *8*, 1341. [CrossRef]
53. Arantes, P.R.; Polêto, M.D.; Pedebos, C.; Ligabue-Braun, R. Making it rain: Cloud-based molecular simulations for everyone. *J. Chem. Inf. Model.* **2021**, *61*, 4852–4856. [CrossRef]
54. Kohout, P.; Vasina, M.; Majerova, M.; Novakova, V.; Damborsky, J.; Bednar, D.; Marek, M.; Prokop, Z.; Mazurenko, S. Engineering dehalogenase enzymes using variational autoencoder-generated latent spaces and microfluidics. *J. Am. Chem. Soc.* **2025**, *5*, 838–850. [CrossRef]
55. Khan, R.T.; Musil, M.; Stourac, J.; Damborsky, J.; Bednar, D. Fully automated ancestral sequence reconstruction using FireProt^{ASR}. *Curr. Protoc.* **2021**, *1*, e30. [CrossRef]
56. Musil, M.; Khan, R.T.; Beier, A.; Stourac, J.; Konegger, H.; Damborsky, J.; Bednar, D. FireProt^{ASR}: A web server for fully automated ancestral sequence reconstruction. *Brief. Bioinform.* **2021**, *22*, bbaa337. [CrossRef]
57. Rambaut, A. *Figtree*, v1.4.3; Institute of Evolutionary Biology, University of Edinburgh: Edinburgh, UK, 2018. Available online: https://beast.community/figtree (accessed on 1 February 2026).
58. Jumper, J.; Evans, R.; Pritzel, A.; Green, T.; Figurnov, M.; Ronneberger, O.; Tunyasuvunakool, K.; Bates, R.; Žídek, A.; Potapenko, A.; et al. Highly accurate protein structure prediction with AlphaFold. *Nature* **2021**, *596*, 583–589. [CrossRef]
59. Pei, J.; Kim, B.-H.; Grishin, N.V. PROMALS3D: A tool for multiple protein sequence and structure alignments. *Nucleic Acids Res.* **2008**, *36*, 2295–2300. [CrossRef]
60. Biasini, M.; Bienert, S.; Waterhouse, A.; Arnold, K.; Studer, G.; Schmidt, T.; Kiefer, F.; Gallo Cassarino, T.; Bertoni, M. SWISS-MODEL: Modelling protein tertiary and quaternary structure using evolutionary information. *Nucleic Acids Res.* **2014**, *42*, W252–W258. [CrossRef]
61. Hekkelman, M.L.; de Vries, I.; Joosten, R.P.; Perrakis, A. AlphaFill: Enriching AlphaFold models with ligands and cofactors. *Nat. Methods* **2023**, *20*, 205–213. [CrossRef]
62. Krieger, E.; Darden, T.; Nabuurs, S.B.; Finkelstein, A.; Vriend, G. Making optimal use of empirical energy functions: Force-field parameterization in crystal space. *Proteins* **2004**, *57*, 678–683. [CrossRef]
63. Krieger, E.; Joo, K.; Lee, J.; Lee, J.; Raman, S.; Thompson, J.; Tyka, M.; Baker, D.; Karplus, K. Improving physical realism, stereochemistry, and side-chain accuracy in homology modeling: Four approaches that performed well in CASP8. *Proteins* **2009**, *77*, 114–122. [CrossRef]
64. Laskowski, R.A.; MacArthur, M.W.; Moss, D.S.; Thornton, J.M. PROCHECK—A program to check the stereochemical quality of protein structures. *J. Appl. Cryst.* **1993**, *26*, 283–291. [CrossRef]
65. Ramachandran, G.N.; Ramakrishnan, C.; Sasisekharan, V. Stereochemistry of polypeptide chain configurations. *J. Mol. Biol.* **1963**, *7*, 95–99. [CrossRef]
66. Volkamer, A.; Kuhn, D.; Grombacher, T.; Rippmann, F.; Rarey, M. Combining global and local measures for structure-based draggability predictions. *J. Chem. Inf. Mod.* **2012**, *52*, 360–372. [CrossRef]
67. Ehrt, C.; Schulze, T.; Graef, J.; Diedrich, K.; Pletzer-Zelgert, J.; Rarey, M. ProteinsPlus: A publicly available resource for protein structure mining. *Nucleic Acids Res.* **2025**, *53*, W478–W484. [CrossRef]
68. Henderson, S.W.; Nourmohammadi, S.; Hrmova, M. Protein structural modelling and transport thermodynamics reveal that plant cation–chloride cotransporters mediate potassium–chloride symport. *Int. J. Mol. Sci.* **2024**, *25*, 12955. [CrossRef]
69. Luang, S.; Fernández-Luengo, X.; Streltsov, V.A.; Maréchal, J.-D.; Masgrau, L.; Hrmova, M. The structure and dynamics of networks underlie catalytic efficiency in a plant glycoside exo-hydrolase. *Commun. Biol.* **2025**, *8*, 729. [CrossRef]
70. Camacho, C.; Coulouris, G.; Avagyan, V.; Ma, N.; Papadopoulos, J.; Bealer, K.; Madden, T.L. BLAST+: Architecture and applications. *BMC Bioinform.* **2009**, *10*, 421. [CrossRef]
71. Thomas, P.D.; Ebert, D.; Muruganujan, A.; Mushayahama, T.; Albou, L.P.; Mi, H. PANTHER: Making genome-scale phylogenetics accessible to all. *Protein Sci.* **2022**, *31*, 8–22. [CrossRef]
72. Liu, X.Q.; Liu, X.P.; Jin, L.; Luo, M.; Tang, Y.J.; Yan, Y.Z.; Duan, C.G.; Zhu, C. A fungal effector inhibits plant MAPK signaling by acting as a decoy substrate of MKK5. *Proc. Natl. Acad. Sci. USA* **2026**, *123*, e2603182123. [CrossRef]
73. Zhang, R.; Tucker, M.R.; Burton, R.A.; Shirley, N.J.; Little, A.; Morris, J.; Milne, L.; Houston, K.; Hedley, P.E.; Waugh, R.; et al. The dynamics of transcript abundance during cellularisation of developing barley endosperm. *Plant Phys.* **2016**, *170*, 1549–1565. [CrossRef]
74. Knudsen, S.; Wendt, T.; Dockter, C.; Thomsen, H.C.; Rasmussen, M.; Jørgensen, M.E.; Lu, Q.; Voss, C.; Murozuka, E.; Østerberg, J.T.; et al. FIND-IT: Accelerated trait development for a green evolution. *Sci. Adv.* **2022**, *8*, eabq2266. [CrossRef]
75. Chan, S.H.S.; Streit, J.O.; Włodarski, T.; Mitropoulou, A.N.; Cassaignau, A.M.E.; Bukvin, I.V.; Waudby, C.A.; Cabrita, L.D.; Christodoulou, J. Structures of protein folding intermediates on the ribosome. *Nat. Struct. Mol. Biol.* **2026**, *33*, 962–972. [CrossRef]

76. Rico-Resendiz, F.; Pri-Tal, O.; Raia, P.; Moretti, A.; Chen, H.; Yu, J.; Broger, L.; Fuchs, C.; Hothorn, L.A.; Loubéry, S.; et al. Plant Kelch phosphatases are Ser/Thr phosphatases involved in cell cycle regulation. *Proc. Natl. Acad. Sci. USA* **2026**, *123*, e2600591123. [CrossRef]
77. Falckenhayn, J.; Kaufmann, R. Current challenges in cryogenic super-resolution fluorescence microscopy in the context of cryogenic electron microscopy/tomography. *Curr. Opin. Struct. Biol.* **2026**, *100*, 103338. [CrossRef]

Disclaimer/Publisher's Note: The statements, opinions and data contained in all publications are solely those of the individual author(s) and contributor(s) and not of MDPI and/or the editor(s). MDPI and/or the editor(s) disclaim responsibility for any injury to people or property resulting from any ideas, methods, instructions or products referred to in the content.